UNIVERSITY OF OKLAHOMA

GRADUATE COLLEGE

A SIMPLE EM DIPOLE RADIATING ELEMENT FOR DUAL-POLARIZED PHASED ARRAY WEATHER RADARS

A THESIS

SUBMITTED TO THE GRADUATE FACULTY

in partial fulfillment of the requirements for the

Degree of

MASTER OF SCIENCE

By

RIDHWAN KHALID MIRZA
Norman, Oklahoma
2016

A SIMPLE EM DIPOLE RADIATING ELEMENT FOR DUAL-POLARIZED PHASED ARRAY WEATHER RADARS

A THESIS APPROVED FOR THE
SCHOOL OF ELECTRICAL AND COMPUTER ENGINEERING

BY

_____
Dr. Yan Zhang, Chair

_____
Dr. Dusan Zrnic

_____
Dr. Jorge Salazar-Cerreño

Acknowledgements

In the name of Allah, the most gracious and the most merciful. Alhamdulillah! All praise be to Allah for the strengths he gave me and the blessings he bestowed upon me in completing this thesis.

I would like to express my sincerest gratitude to my advisor, Dr. Yan Rockee Zhang. Without his inspiration, guidance, support and encouragement this thesis would not have been possible.

I am also thankful to my committee members and advisors Dr. Dusan Zrnic, Dr. Richard Doviak and Dr. Jorge Salazar for guiding me, teaching me and sharing their knowledge and experience with me.

I also thank my parents and my family for their encouragement who are so supportive throughout my life.

Last but not least, I would like to thank all the people who have helped me during the research and all my friends in ARRC: Ramesh Nepal, Sudantha Perera, Xining Yu and Jingxiao Cai.

Table of Contents

List of Tables

List of Figures

Abstract

The Dual Polarized radiating element is a critical component in the Multi-function Phased Array Radar (MPAR) System. This thesis studies a new type of dual polarized radiating element based on the Electro-Magnetic (EM) dipole concept. Two different geometries i.e., loop approximated as magnetic dipole and a printed electric dipole are used to form a single dual polarized radiating element. Radiation patterns based on Ansoft® High Frequency Structural Simulator (HFSS) simulation software and measurements carried out in Anechoic Chambers are presented. The results are compared to commercially available electric and magnetic dipole antennas. An Initial array and simple linear array design based on these elements is also discussed.

Chapter 1: Introduction

In recent years, Multi-function Phased Array Radars (MPAR) has received more attention due to their ability to perform multiple functions such as aircraft tracking and weather surveillance. The MPAR is being considered for fulfilling the need of FAA, NOAA/NWS and possibly Homeland Security [1]. One of the specific goals of deploying MPAR systems is to replace the current Weather Surveillance Radar (WSR-88D radar) [2].

In many radar applications and weather radar polarimetry, the physical symmetry of the target and weather scan moments can be detected by phased array antennas which require suppression of antenna cross polarization (X-pol) especially during the main beam shift or scanning off-broadside direction [3, 4]. The current state of art parabolic reflector antennas which are used for weather surveillance are required to scan mechanically and lack the ability to scan the beam electronically in contrast to phased array radars. The cross polarization(X-pol) factor of phased array radar can be minimized effectively if the single antenna element is designed in such a way that the X-pol factors for each antenna unit is minimum at all scan angles.

Dual Polarized Antenna elements when used for phased array radars and especially weather radar systems, have an advantage of polarization diversity. That is, by using a single dual polarized antenna, two different signals can be transmitted or received without any extra bandwidth requirement or physical separation between antennas. This dual polarized element provides the ability to observe backscattering from targets (precipitation, clutter etc.) in the form of horizontally and vertically

polarized electromagnetic waves. For instance, vertical tree trunks and structures can be tracked by HH polarization. VV polarization can provide water and soil scattering information [5]. However, for accurate polar metric measurements it is required for the antenna to have high cross polarization suppression. The cross polarization isolation as required by many weather polarimetry applications is less than 20 dB for alternate transmission and less than 40 dB for simultaneous transmission and reception [2, 6].

Most of the existing efforts in MPAR radiating elements are based on microstrip patch antenna elements [4, 7, 8]. Although better than -30 dB cross pol levels are achieved in most of the rectangular patch-based MPAR sub-array prototypes, certain challenges arise when steered-beam calibrations are needed for precise dual-pol measurements. The fundamental problem in these designs is that the relationships between co and cross-pol electric fields are not consistent for different antenna pointing angles especially when scanning off-broadside direction [8]. Theoretically, an ideal radiating element should radiate orthogonal co-polar fields in all spatial directions for two different polarizations [2, 9]. To achieve this two types of dual polarization elements are considered. The first one is a pair of orthogonal or cross dipole element configuration in which the electric fields are orthogonal only in principal planes which is under investigation by many researchers [10-12]. The other type of radiator is a pair of magnetic dipole and electric dipole for which the electric fields are orthogonal in all spatial directions. The latter configuration is investigated and proposed in this thesis as the dual polarized radiating element.

There are other important advantages of using dipole elements in MPAR type systems, especially in Cylindrical Phased Array Radars [8], since using discrete dipole

elements can effectively avoid surface and travelling wave propagations. Currently, the main challenges of applying dipole elements are higher costs for fabrication and potential requirements of 3-dimensional structures.

Initial implementations of such dipole configuration have been made by the industry (Lockheed Martin and BCI). This is realized in the form of slot which acts as a magnetic dipole and the electric dipole is in the front of the slot as seen in Figure 1.

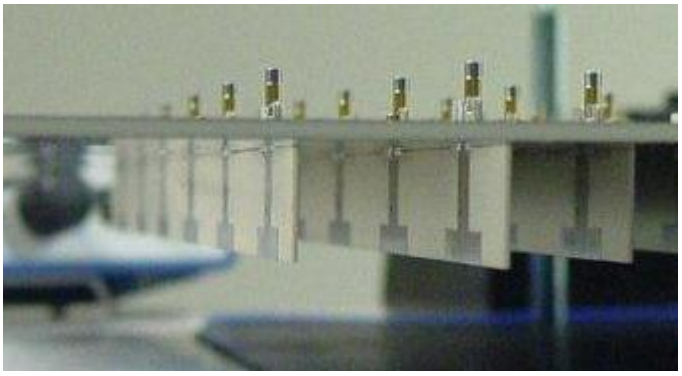

(a)

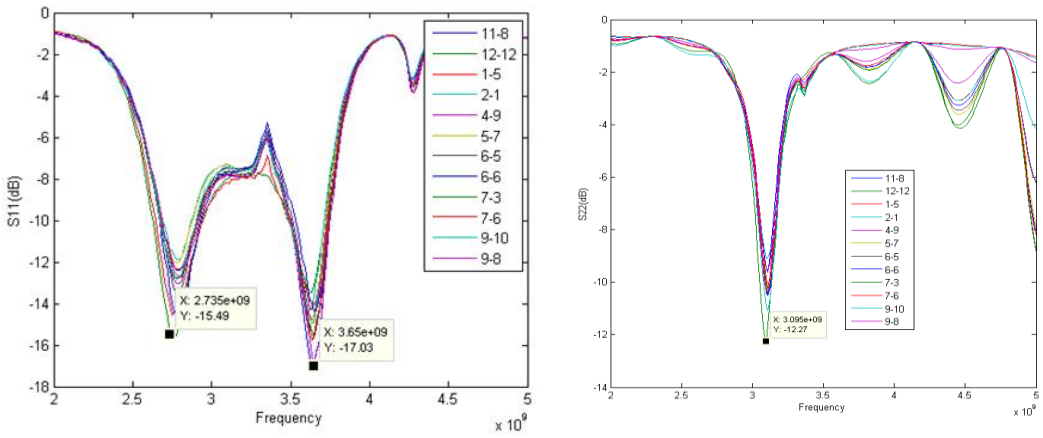

(b) (c)

Figure 1: Slot-dipole array (Lockheed Martin and BCI Corp.)
(a) Top view of the array (b) S_{11} (dB) for electric dipole (c) S_{22} (dB) for slot

However, the individual operating frequencies for slot and dipole of this array differ and the blockage of slot by dipole is evident. The Figure 1(b) shows that electric dipole operates at 2.7 GHz and 3.6 GHz whereas the slot resonates at 3 GHz as seen in Figure 1(c). This means that slot and electric dipole of this array do not have a common operating frequency. Hence, much more work remains to be done to achieve a realistic, low-cost and well performing engineering design. The goal of this thesis is to propose new radiating elements (in contrast to conventional microstrip elements) for Phased Array Radars on which future research can be conducted.

1.1 Overview of the Thesis

In this thesis, a pair of electric and magnetic dipole is proposed to serve the purpose of a dual polarized element. The Chapter 2 gives a brief introduction to the basic antenna theory and definitions. The Chapter 3 details about a basic loop structure and its requirement to achieve a characteristics of a magnetic dipole. To achieve this various design with different types of feeding is investigated, out of which the loop with capacitive loading achieves a pattern which is close to an ideal magnetic dipole. The Chapter 4 is concerned with design of a printed dipole. The simulation results for these designs are discussed. Next, Chapter 5 shows the electric field equations and duality principle applied to magnetic and electric dipole which leads to formation of a dual polarized radiating element. Lastly, the Chapter 6 and Chapter 7 shows the setup, procedure and measurement results carried out in anechoic chambers.

Chapter 2: Background

This chapter describes the basic theory on the electromagnetic fields, antenna co-ordinate system, and basic definitions used in this thesis. Some basic theory about loop antenna, electric dipole, electromagnetic radiation and their characteristics as compared to its counter parts are also discussed.

2.1 Electromagnetic Radiation Field Regions

The antenna radiation is described in terms of electromagnetic field radiation. The space surrounding any antenna is divided into three regions based on the distance from the antenna under test (AUT). These regions are based on equations as described in the table below [9].

Region	Distance
Near-Field or Reactive Near Field Region	$0 < r < 0.62\sqrt{\frac{D^3}{\lambda}}$
Reactive Near-Field or Fresnel Region	$0.62\sqrt{\frac{D^3}{\lambda}} \leq r \leq 2\frac{D^2}{\lambda}$
Far-Field or Fraunhofer Region	$2\frac{D^2}{\lambda} \leq r$

Table 1: Different field regions surrounding an antenna

As seen in the above Table 1 these regions are classified based on the above equations where 'r' is the distance from the source or AUT, 'D' is the maximum dimension of the AUT and 'λ' is the wavelength of the radiation. The field region of antenna is important in terms of measuring several parameters discussed in this thesis.

Most of the times the targets are placed or objects are measured in the Far-Field or Fraunhofer Region. These regions are also illustrated in the Figure 2 shown below

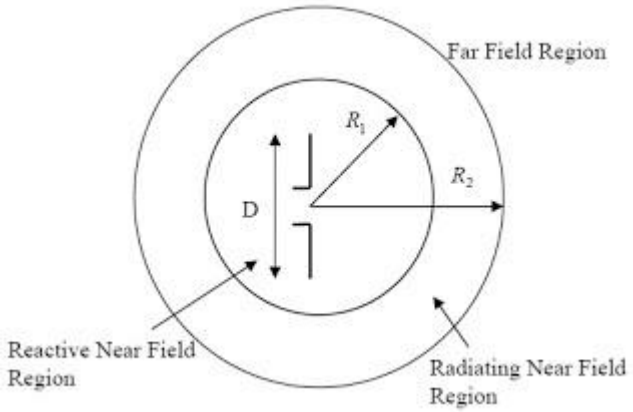

Figure 2: Field regions surrounding an antenna

2.2 Antenna Co-ordinate System

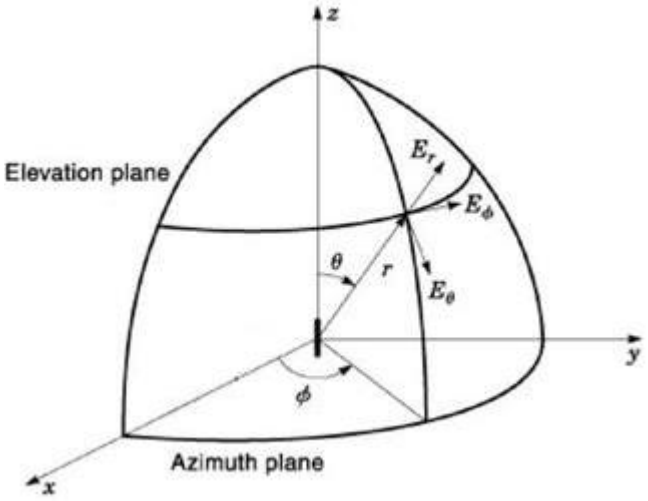

Figure 3: Spherical coordinate system used for antenna analysis[9]

The characteristics of an antenna are graphically represented by its radiation pattern. The radiation pattern is mostly determined in far-field region and illustrated using the spherical co-ordinate system as shown in the Figure 3. In this system the antenna is placed at the origin and '*r*' is the distance or radius from the AUT to the observation

point. The radiation properties of an AUT is determined by varying the elevation or zenith angle 'θ', azimuth angle 'ϕ' and field vectors E_θ, E_ϕ are calculated. This spherical co-ordinate system is used in this thesis for simulation and carrying out measurements in the anechoic chambers. More information on the spherical co-ordinate system used in anechoic chamber is discussed in Chapter 6 of this thesis.

2.2 Antenna Polarizations

The polarization of the radiated electric fields produced by an antenna in a given direction is referred as polarization of an antenna. There are several ways in which antenna can be polarized, such as linear polarization, circular polarization, left hand polarization, right hand polarization and elliptical polarization [9].

However in weather radar polarimetry, the most important property concerned is the co-polarization (often called as co-pol) and cross-polarization (often called as cross-pol or X-pol) of a radiating element. The term co-polarization is the desired polarization component of the radiation pattern and cross-polarization is the unwanted component of radiation pattern. For instance, if the transmitting antenna is meant to transmit horizontally polarized waves and the receiving antenna on the other end is receiving horizontally polarized waves, it is said to receive co-pol radiation or desired radiation. On the contrary if the receiving antenna was supposed to receive vertically polarized waves, it is receiving cross-polarization or unwanted radiation.

There are three most widely used definitions for cross-pol and co-pol as given by Ludwig [13]. For weather radars, the second definition of Ludwig (L2) is widely accepted to define the co and cross polarizations.

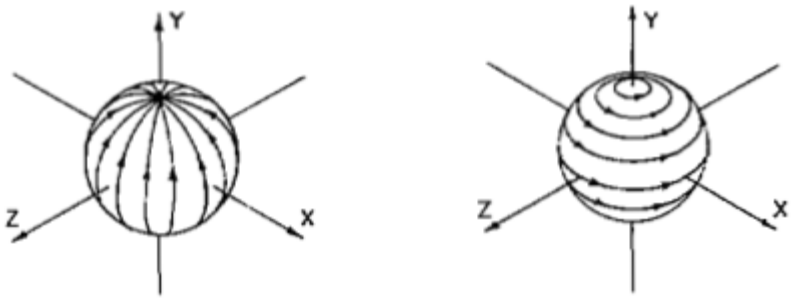

(a) (b)

Figure 4: Ludwig II co-ordinate system [13]
(a) Direction of reference polarization (b) Direction of cross polarization

According to Ludwig's second definition [13], we have

$$\hat{\imath}_{ref} = \frac{sin\phi cos\theta\, \hat{\imath}_\theta + cos\phi \hat{\imath}_\phi}{\sqrt{1 - sin^2\theta sin^2\phi}} \quad (1)$$

$$\hat{\imath}_{cross} = \frac{cos\phi \hat{\imath}_\theta - cos\theta sin\phi \hat{\imath}_\phi}{\sqrt{1 - sin^2\theta sin^2\phi}} \quad (2)$$

Where $\hat{\imath}_{ref}$ and $\hat{\imath}_{cross}$ are the projections of electric field vectors onto spherical unit vectors given by Ludwig [13] such that,

$E.\hat{\imath}_{ref}$= the reference polarization (co-pol) component of E

$E.\hat{\imath}_{cross}$= the cross polarization (cross-pol) component of E

The spherical coordinate system used for the weather radar polarimetry and most of the standard antenna measurements is as depicted in Figure 3, in which the polar axis is along z axis and antenna axis is aligned along z axis. After this the Ludwig's II definition (transformation) is applied to obtain the co-polar and cross-polar patterns. Hence, all the measurements shown in this thesis will be as per L2 definition

of cross polarization, and the measurement setup for OU's anechoic chamber will be discussed in Chapter 6.

2.3 Antenna Types

Among different types of antennas like wire antennas, aperture antennas and microstrip antennas, the microstrip antennas are becoming very popular due to the variety of applications in government and commercial sectors [9]. The main advantage of these microstrip antennas is the minimum size and space requirements as compared to its counterparts like horns, waveguides etc. Other factors such as low cost, light weight and ease of fabrication make these types of antennas suitable for building an array. The microstrip antenna consists of a simple dielectric substrate on one side and a radiating metallic surface on the opposite side as shown in Figure 5.

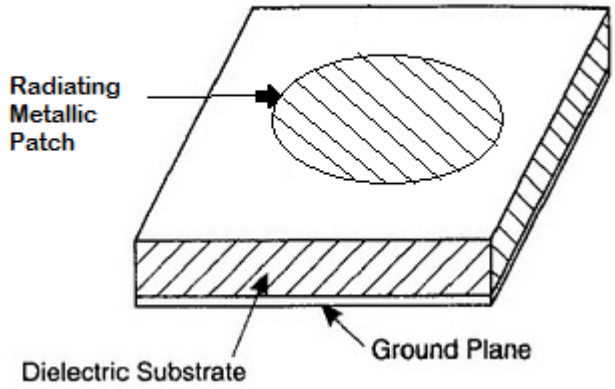

Figure 5: Microstrip antenna

The radiating metallic patch can take different forms like rectangular patch, circular loop, triangular, dipole, etc. Most of the microstrip antennas are designed such that they radiate from the top metallic layer is maximum along normal (broadside radiation). The dielectric is chosen from a variety of thin and thick substrates with

dielectric constants ranging between $2 \leq \varepsilon_r \leq 12$. There are also different feeding techniques for microstrips and the most popular are microstrip line, coaxial probe, aperture coupling and proximity coupling [9]. In this thesis, the microstrip antenna takes the form of a loop and a printed electric dipole. The feeding techniques and design of these structures are discussed in the next following Chapters.

Chapter 3: Loop as Magnetic Dipole

Loop Antennas as discussed in Chapter 2 is one of the inexpensive, simple and versatile forms of microstrip antenna. In this Chapter, the basic requirement for a loop to exhibit magnetic dipole characteristics and different implementations of loop antennas will be discussed. It will be shown that a loop antenna with capacitive loading has uniform current distributions and its simulation results are discussed.

3.1 Magnetic Fields Due to Constant Current Loop

A loop having a constant current along its circumference can be said to have the same fields as compared to that of a magnetic dipole. To illustrate this, consider a loop with constant current 'i', radius 'r', and an observation point at a far field distance 'R' as shown in Figure 6. At far field distance where ($R \gg r$), the loop can be treated as a small circular loop with constant current and the calculation of magnetic field depends on the current 'i', 'R' and 'θ' i.e., the angle form the Z-axis. The magnetic field equations are given by [14]

$$B = \begin{cases} B_r = 2|\mu|\mu_0 \frac{cos\theta}{4\pi R^3} \\ B_\theta = |\mu|\mu_0 \frac{sin\theta}{4\pi R^3} \end{cases} \qquad (3)$$

Where $\mu = iA$ is the magnetic dipole moment of the loop and 'A' is the area of the loop. These magnetic fields produced by the loop are equivalent to the fields produced by a small magnetic dipole. The magnetic dipole moment as stated above is a vector pointing out normal to the plane of the loop and its magnitude is equal to the product of current and area of the loop.

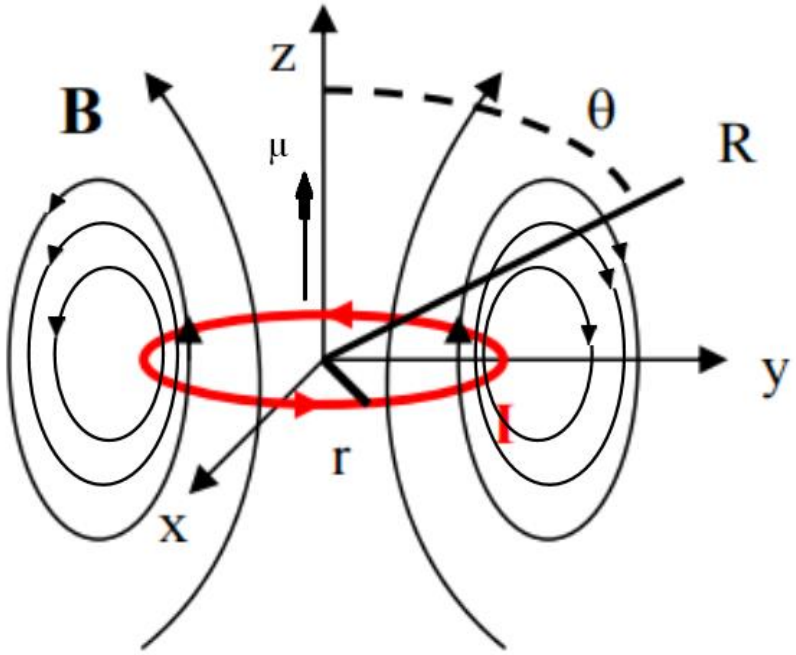

Figure 6: Illustration of magnetic fields around a loop

3.2 Initial Implementations and Simulations with Loop Antennas

At the elementary stages of research for this thesis, initial loop antennas were simulated based on the cavity theory model [15] and spectral domain moment methods [16]. These included coax fed single layer loop and coax fed multi-layered stacked loop as shown in Figure 7. The resonant frequency is obtained as

$$f_{mn} = \frac{X_{nm}c}{2\pi a\sqrt{\varepsilon_{re}}} \qquad (4)$$

where c= velocity of light in free space

a= inner radii of the ring

b= Outer radii of the ring

ε_r= dielectric constant of the substrate

$\varepsilon_{re} = \frac{1}{2}(\varepsilon_r + 1) + \frac{1}{2}(\varepsilon_r - 1)\sqrt{(1 + \frac{10h}{W})}$;

$W = b - a$

$X_{nm} = k_{mn}a$; h= thickness of dielectric

k_{mn} are the roots for the resonant TM_{nm} modes and are not discussed for the sake of brevity.

Single Layer Loop	Multi-Layer Stacked Loop
Inner Radius=16.902mm; Outer Radius =33.804mm	Lower Layer: Inner Radius=10mm Outer Radius= 29mm
Substrate: Rogers 5880 with $\varepsilon_r = 2.33$ and substrate thickness h=6.096mm.	Lower Layer Substrate: $\varepsilon_r 1$=2.2 with tanδ1=0.001 and thickness h=6.096mm
	Top Layer: Inner Radius=14mm Outer Radius=31mm
	Lower Layer Substrate: $\varepsilon_r 2$=2.107 with tanδ2=0.001 and thickness h=8mm

Table 2: Design parameters for loops

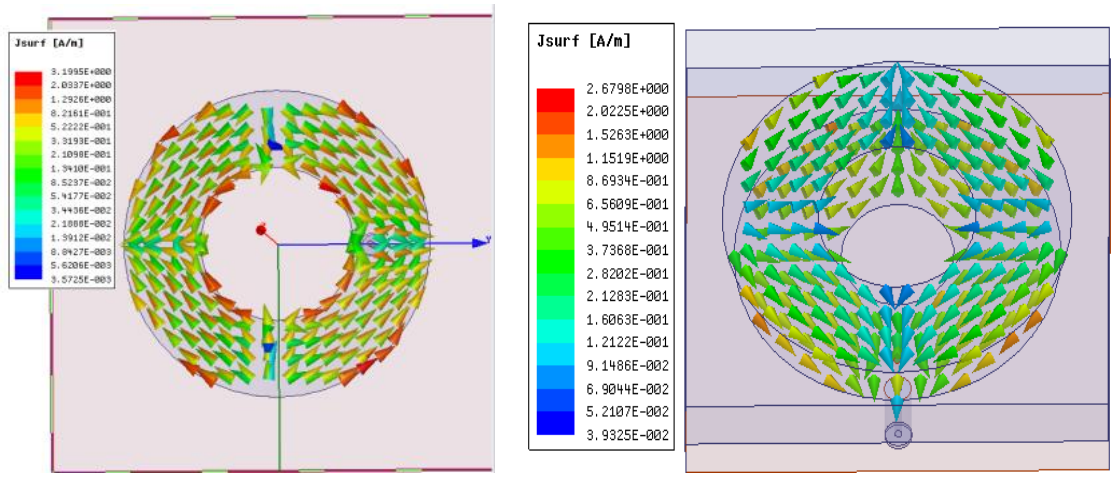

(a) **(b)**

Figure 7: Initial loop antenna implementations (a) Single layer coax fed loop (b) Multi-layered stacked loop with coax feed

The probe feed is located based on trial and error method to get the best matching results and where the return loss S_{11} is lowest. The single layer loop was simulated using Rogers 5880 material and the multi-layered loop had two dielectrics

with ε_r1=2.2, ε_r2=1.07, tanδ1=0.001, tanδ2=0.001. The design and simulation results are not discussed in detail in this thesis for the sake of conciseness. These results are published in a conference paper and can be found in [17].

However, for any loop or ring antenna to preserve the characteristics of a magnetic dipole, it is required that the surface current on the surface of the loop must be in phase and constant. Although the matching and other radiation characteristics seems convincing [17], but it can be seen in Figure 7 that the current direction is not uniform which makes it different from the ideal magnetic loop dipole as discussed in section 3.1.

3.3 Design and Simulation Results of Loop based on Capacitive Loading

As discussed in section 3.1 and 3.2, a loop antenna should have uniform uni-directional current to retain the characteristics of a magnetic dipole. This is generally difficult to achieve for smaller loop antennas because of high reactance and small radiation resistance which leads to improper matching [9, 18]. To combat this problem, the idea of driving the loop currents in segments was first introduced by Foster [19] which also explains the analytical solution for radiation resistance and directivity for these type of loops. Later Li et al [20] proved that by adding a capacitive reactance on the loop at every 45˚, a uniform travelling wave current distribution can be obtained. A similar approach was considered by Wei [21] for designing a horizontally polarized loop antenna. The loop antenna shown in Figure 8 is reproduced using the original design by Wei [21] with different substrate material and different operating frequencies.

This proposed loop shown in Figure 8 has periodic capacitive loading at every 45˚ and consists of strip-line sections which are similar to unit cell described by Park [22]. This unit cell which is periodically placed helps to create a series capacitance and

allows the surface current distribution to be uni-directional and uniform in phase, as seen in Figure 8(b). Therefore, this antenna can be considered as magnetic dipole in far-fields.

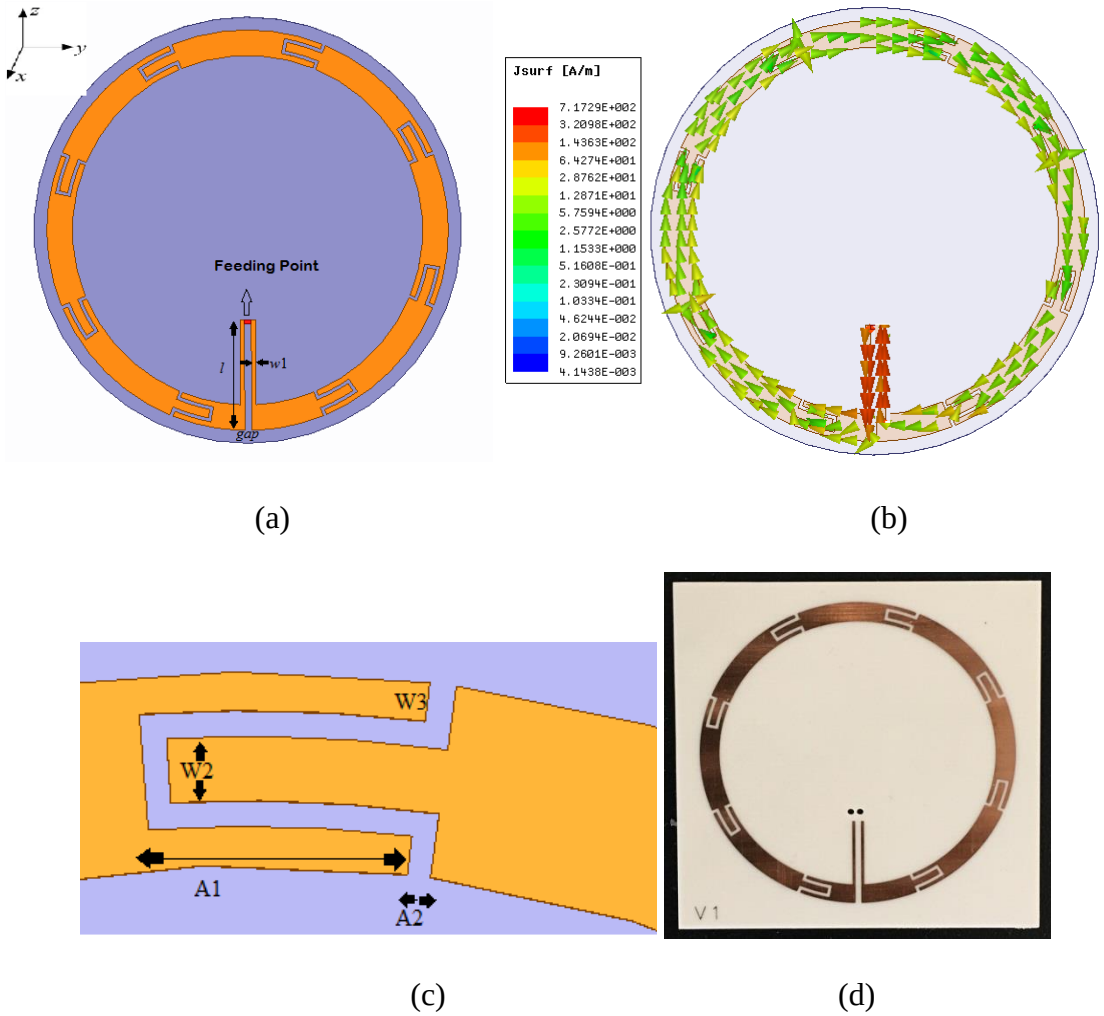

Figure 8: Loop with capacitive loading (a) Design in HFSS (b) Illustration of surface current (c) Dimensions of the unit cell (d) Fabricated prototype

The dielectric substrate used is Rogers 4725JXR (ε_r=2.64) with 1 oz copper and 0.787 mm thickness. The loop has outer radius (R1) =23.5 mm, inner radius (R2) =20.5 mm. The periodic unit strip line sections are place at every 45˚. Each unit cell of strip line has the following dimensions as depicted in Figure 8(c) as A_1=11˚ or 4 mm, A_2=1˚ or 0.35 mm, w_2=1 mm, w_3=0.6 mm. The number of unit cells for capacitive

loading are related by relation $A_1+A_2=\frac{360}{N}$, where N being the number of unit cells. Another advantage of using the periodic capacitive loading is to achieve a wide impedance bandwidth [21]. The antenna is fed by using a parallel strip-line which is a balanced structure and also plays a role of a balun and helps in maintaining impedance matching. Each strip-line has a length (l) = 13 mm, width (w_1) = 0.5 mm and gap = 0.8 mm as seen in Figure 8(a).The loop antenna is designed in Ansoft HFSS simulation software. The antenna is excited by using lumped port excitation and Absorbing Boundary Conditions (ABC) was used in the simulation environment. The ABC boundaries are placed at a distance more than $\frac{\lambda}{4}$ from the antenna.

The fabricated prototype is shown in Figure 8(d). The antenna is fed using a twin lead cable. The return loss (S_{11}) is measured using the PNA and can be seen in Figure 9(a). The antenna is designed to operate over 2.3 GHz to 3.1 GHz in simulation. However the measured results show that antenna has good return loss over 2.5 GHz to 3.0 GHz which gives us at least about 500 MHz of bandwidth.

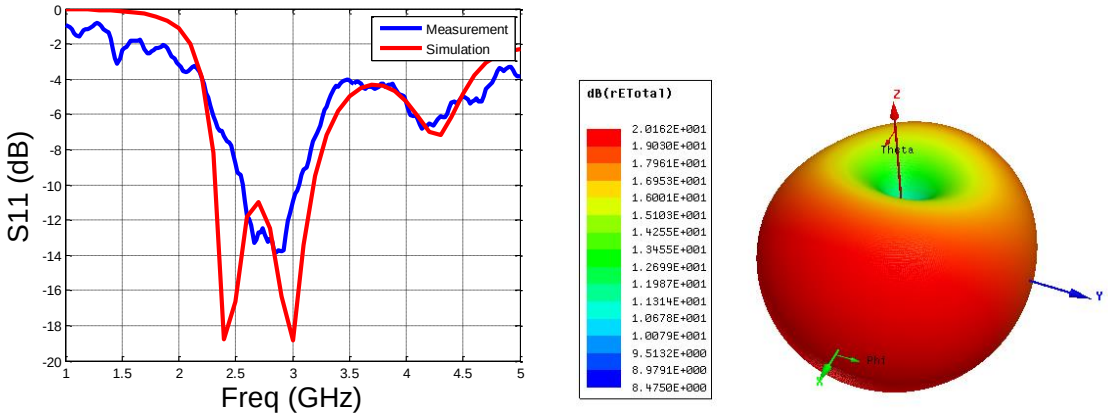

(a) (b)

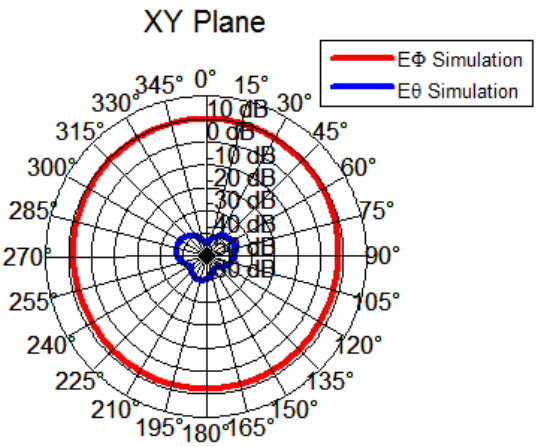

(c)

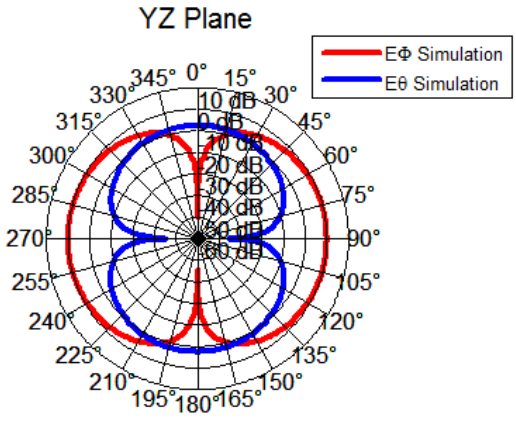

(d)

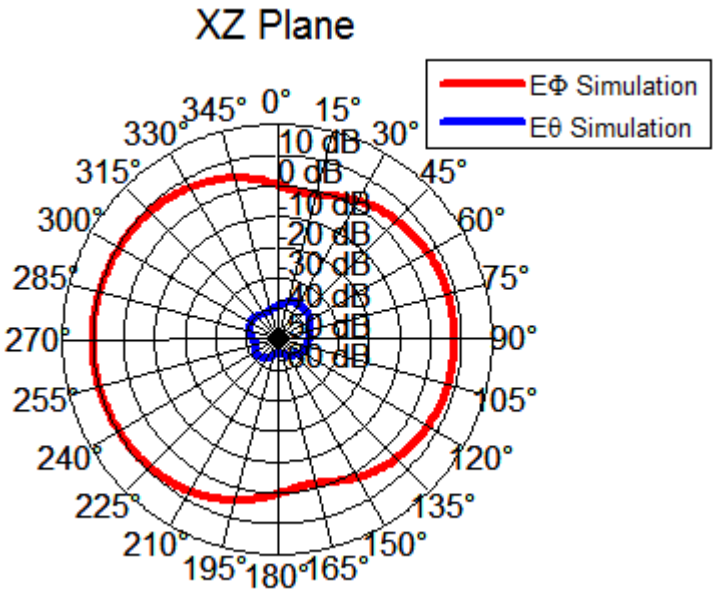

(e)

Figure 9: HFSS simulated return loss and radiation patterns of the loop antenna (a) Return loss (S_{11}) in dB (b) Total 3D radiation pattern (c) XY plane cut of the radiation pattern (d) YZ plane cut of the radiation pattern (e) XZ plane cut of the radiation pattern

The radiation patterns in principal planes are displayed in Figure 9 for the loop antenna simulated at 2.8 GHz. Since the loop is horizontally polarized, it is meant to radiate horizontally polarized fields (E_ϕ i.e., co-polar radiation for this case). However,

there are also vertically polarized fields (E_θ i.e., the cross-polar radiation for this case) which arise due to unwanted electric fields (orthogonal to desired direction) from the loop, feeding point and material imperfections. It can be observed that the radiation fields of the loop are close to an ideal magnetic dipole as it exhibits a pattern similar to that of a doughnut shape with a null along its axis (in elevation plane) and has maximum radiation along the plane of the loop (XY-plane). Ideally, for a magnetic dipole, the radiation in XZ plane and YZ plane should be similar. However, because of the feed line design of this loop, there is some electric field radiation from this feed line (two parallel strip lines). This adds up to the cross polar fields and constitutes stronger E_θ in YZ plane. The results of the fabricated prototype of Figure 8(d) will be discussed in Chapter 7 and will be compared with other commercially available magnetic dipoles.

Chapter 4: Printed Electric Dipole

An Electric Dipole antenna is considered as one of the simplest form of linear wire antennas and widely used for many applications [23]. The basic construction of dipole is straightforward. A simple linear wire dipole consists of a conductor (wire) which is split in middle to allow the feeder to transmit or receive power.

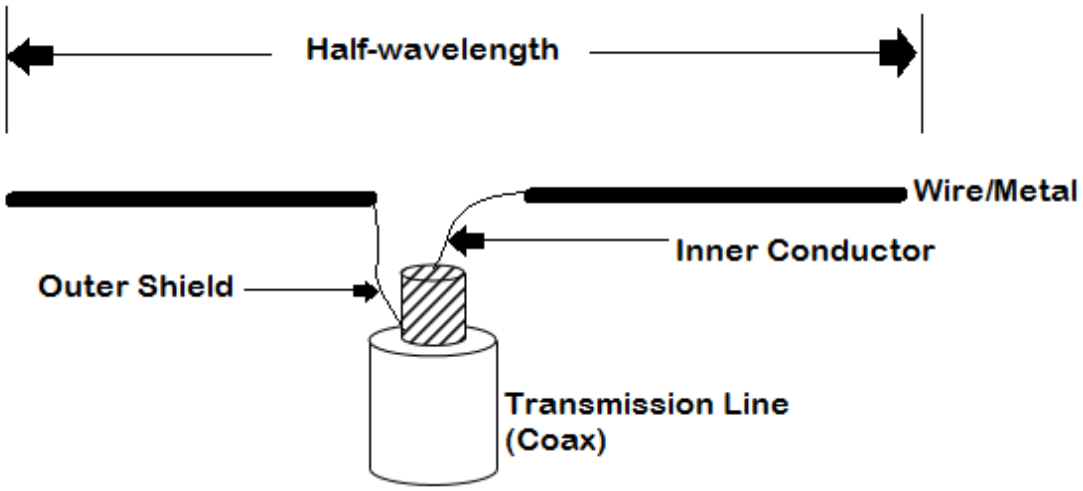

Figure 10: A simple linear wire dipole antenna

As shown in Figure 10, a dipole consists of two poles, the length of each pole is quarter wavelength ($\frac{\lambda}{4}$), thereby making overall dipole as half-wavelength ($\frac{\lambda}{2}$).The dipole radiates equal power in all azimuthal directions perpendicular to the axis of the antenna. Section 4.1 describes the design and simulation of the dipole used in for this research.

4.1 Design and Simulation Results of a Printed Electric Dipole

There are several different variations of dipoles such as wire dipole, folded dipole, printed dipole, cage dipole, bow-tie and batwing antenna [23]. These are specific to the type of application and decisions of design. In this thesis, the printed dipole is

chosen among different variations of dipole antennas, because it is easy to design and does not involve 3-D structures. The advantage of small size, light weight and planar form of dipole can be realized when it is aligned with loop which will be discussed in Chapter 5.

The proposed design in thesis is a very simple planar printed electric dipole. This microstrip dipole antenna has two arms or poles as shown in Figure 11. Each of the arms has length '*L*', width '*W*' and are separated by a gap '*Gap*'.

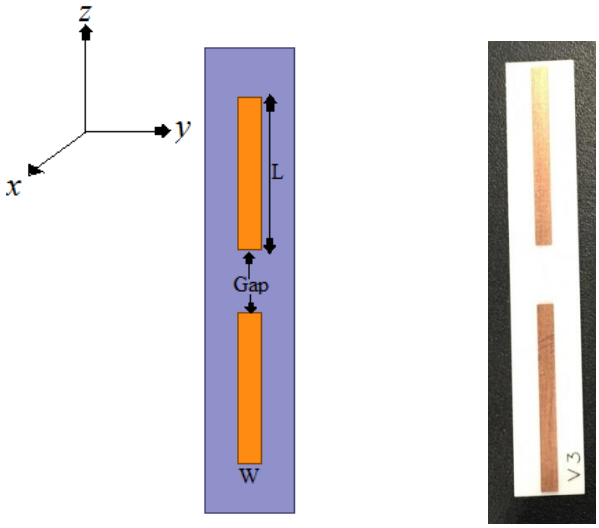

(a) (b)

Figure 11: A printed dipole (a) Design and HFSS model (b) Fabricated prototype

The microstrip printed dipole is implemented on Rogers 4725JXR (ε_r=2.64) with 1 oz copper and 0.787 mm thickness. The design variables are related to each other by the formulae given [24]

$$\varepsilon_e = \frac{\varepsilon_r+1}{2} + \frac{\varepsilon_r-1}{2}\left[\frac{1}{\sqrt{1+12d/W}}\right] \qquad (5)$$

Where

ε_r=Dielectric Constant
ε_e= Effective Dielectric Constant

d= substrate thickness
W= width of microstrip line

The length L of the printed dipole is approximated to quarter wavelength ($\frac{\lambda}{4}$) and the entire dipole constitutes half-wavelengths ($\frac{\lambda}{2}$). The value 'λ' is given by

$$\lambda = \frac{c}{f\sqrt{\varepsilon_e}}$$

where

λ= wavelength
c= velocity of light
f= frequency

The values used for the above fabricated prototype are *L*=17 mm, *W*=2.5 mm, and *Gap*=7 mm. These values are tuned and approximated by using the parametric setup in HFSS simulation software. The antenna is excited by lumped port excitation in HFSS and Absorbing Boundary Conditions (ABC) was used in the simulation environment. The ABC boundaries are placed at a distance more than $\frac{\lambda}{4}$ from the antenna.

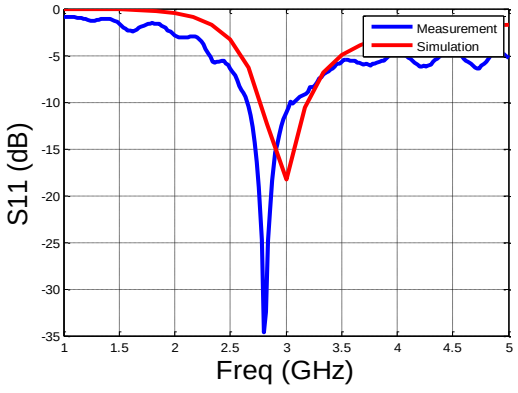

(a)

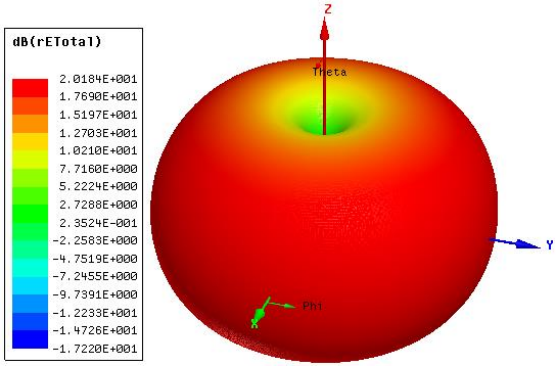

(b)

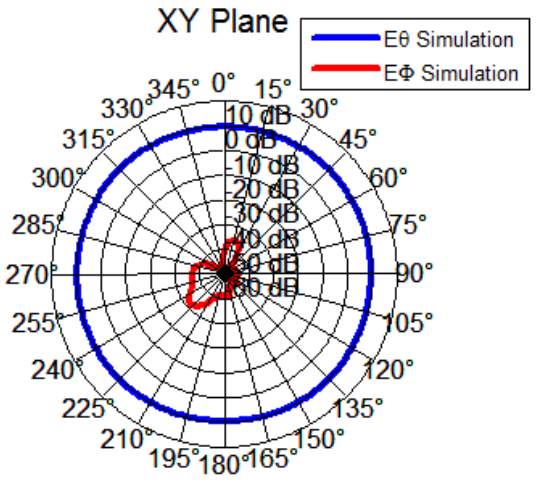

(c)

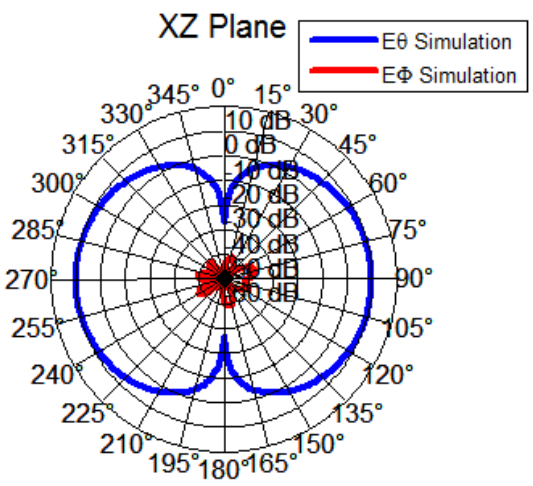

(d)

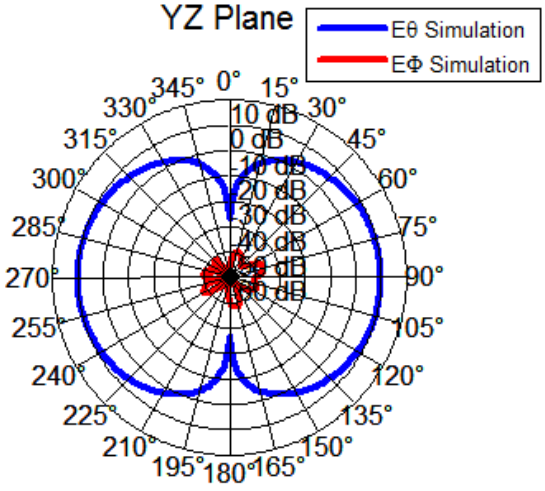

(e)

Figure 12: HFSS simulated return Loss and radiation patterns of the proposed electric dipole antenna (a) Return loss (S11) in dB (b) Total 3D radiation pattern (c) XY plane cut of the radiation pattern (d) XZ plane cut of radiation pattern (e) YZ plane cut of radiation pattern

The electric dipole is designed to operate over 400 MHz bandwidth ranging from 2.7 GHz to 3.1 GHz. However, we see in Figure 12(a) that measurement results show a slight shift in frequency as compared to the simulation. This might be due to the effect of use of the twin lead cable as shown in Figure 10 practically, versus an ideal 50

Ω matched lumped port in simulation. The radiation patterns shown for electric dipole are simulated at 2.8 GHz (selected for the convenience of comparing them with measurement results of electric dipole and loop to be shown in Chapter 7) for principal planes seen in Figure 12. Although, the electric dipole is vertically polarized and it is designed to radiate vertically polarized fields (E_θ i.e., the co-polar radiation for this case) there are also horizontally polarized fields (E_ϕ i.e., the cross-polar radiation) radiated from the antenna. The reason for this cross polar radiation might be due to the factors like antenna aperture, radiation of electric field in unwanted direction (orthogonal to desired direction), material imperfections and radiation from the feed point. The simulation results show that the plane of maximum radiation is in XY plane and there is a null along Z axis which is part of the doughnut shape as seen in Figure 12(b). The results of the fabricated prototype of Figure 11(b) will be discussed in Chapter 7 and will be compared to other commercially available electric dipoles.

Chapter 5: Dual Polarized E&M Dipole Radiating Element

This Chapter describes the theory of radiated fields for loop and electric dipole. The EM dipole arrangement will be discussed and the theory will be proved by showing the HFSS simulations.

5.1 Radiation Fields of Loop Antenna and Electric Dipole

As discussed in Chapter 3, the loop antennas has the same desirable characteristics as to that of a magnetic dipole. The proposed design of the loop as in Chapter 3 is an electrically-large loop as circumference of loop is greater than one-tenth of wavelength (λ/10). But at a far field distance from the source ($R \gg r$), where 'R' is the observation point and 'r' is the radius of the loop, the loop can be considered as an electrically small loop. This electrically small loop antenna acts as a dual antenna to a short dipole antenna. The far-field electric and magnetic fields of magnetic dipole (loop) are identical to the far-field magnetic and electric field of electric dipole respectively [25]. This can be illustrated by considering the Figure 13 [25] below

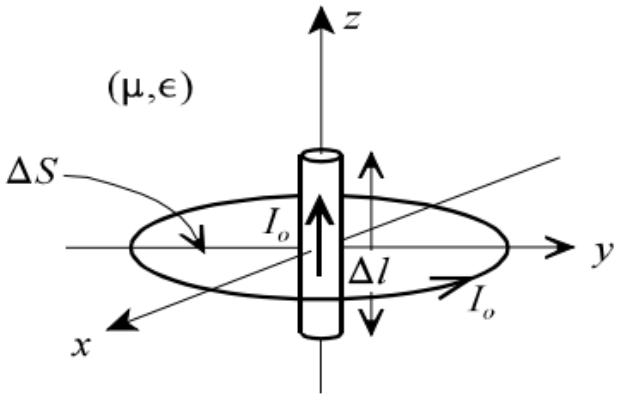

Figure 13: Illustration of loop and electric dipole [25]

Consider a loop having a uniform current 'I_0', area 'ΔS'. The far-field vector potential for electrically small loop is given by [9, 25] as

$$A \approx j\frac{k\mu I_o \Delta S}{4\pi r} e^{-jkr} sin\theta \; a_\phi \qquad (6)$$

Where $\Delta S=\Delta l^2$ i.e., the area of the loop and a_ϕ is the spherical coordinated vector given by $a_\phi = (-sin\phi a_x + cos\phi a_y)$.

The corresponding far field components for electrically small loops can be calculated using equation 4 as [9, 25]

$$E_\phi \approx -j\omega A_\phi \approx \frac{\eta k^2 I_0 \Delta S}{4\pi r} e^{-jkr} sin\theta \qquad (7)$$

$$H_\theta \approx j\frac{\omega}{\eta} A_\phi \approx -\frac{k^2 I_0 \Delta S}{4\pi r} e^{-jkr} sin\theta \qquad (8)$$

If carefully observed, these components are similar to the fields those radiated by an infinitesimal electric dipole [9, 25]. The Table 3 below shows the comparison between these two antennas:

Infinitesimal Electric Dipole	**Electrically Small Loop**
$E_\theta \approx j\frac{\eta k I_0 \Delta l}{4\pi r} e^{-jkr} sin\theta$	$E_\phi \approx \frac{\eta k^2 I_0 \Delta S}{4\pi r} e^{-jkr} sin\theta$
$H_\phi \approx j\frac{k I_0 \Delta l}{4\pi r} e^{-jkr} sin\theta$	$H_\theta \approx -\frac{k^2 I_0 \Delta S}{4\pi r} e^{-jkr} sin\theta$

Table 3: Comparison of far-field elements generated by small electric dipoles and loops

The above equations in Table 3 share the same mathematical forms and it is possible to find the pair of equivalent and dual sources by a systematic interchange of

symbols. This is known as duality theorem [9]. By duality theorem we have dual quantities of electric and magnetic current sources as shown in Table 4.

Electric Source	Magnetic Source
E	H
H	-E
I_o	I_{om}
K	k
H	$\frac{1}{\eta}$

Table 4: Dual quantities for electric and magnetic current sources

Now by applying the above dual quantities, the far-field components of the magnetic sources can be determined and are shown in Table 5.

Infinitesimal Magnetic Dipole	Electrically Small Loop (Magnetic)
$H_\theta \approx j\frac{kI_{0m}\Delta l}{\eta 4\pi r}e^{-jkr}sin\theta$	$H_\phi \approx \frac{k^2 I_{0m}\Delta S}{\eta 4\pi r}e^{-jkr}sin\theta$
$E_\phi \approx -j\frac{kI_{0m}\Delta l}{\eta 4\pi r}e^{-jkr}sin\theta$	$E_\theta \approx \frac{k^2 I_{0m}\Delta S}{\eta 4\pi r}e^{-jkr}sin\theta$

Table 5: Far-field components of corresponding magnetic sources

Therefore, if an electrically small magnetic loop and an electric dipole are designed such that

$$I_o\Delta l = j\eta k I_{om}\Delta S = j\omega\mu I_{om}\Delta S \qquad (9)$$

then due to this equivalence condition, the far fields radiated by the electrically small magnetic loop and electric dipole are equivalent dual sources. Since, these antennas act as dual to each other, the power radiated by both should be same when currents and dimensions are appropriately designed.

5.2 Antenna Arrangement and Polarization

From the above theory, it is important to determine the antenna arrangement which will be used in this thesis for simulations and measurements. In theory, an electrically small loop (magnetic dipole) and an electric dipole are dual antennas to each other, their far-fields are orthogonal to each other if these antennas are aligned as shown in Figure 13. The plane of maximum radiation for the loop and the electric dipole is XY plane; A combination of E&M dipoles is oriented such that the electric field of electric dipole (E_θ) is orthogonal to the electric field of the loop (E_ϕ) everywhere. In other words it can be said as electric dipole should be vertically polarized and loop should be horizontally polarized as shown in Figure 14(a). This can also be illustrated by considering a sphere consisting of latitudes and longitudes. The directions of the fields generated by a loop (magnetic dipole) can be approximated by latitude lines, whereas the direction of the fields generated by electric dipole can be approximated by longitude lines (Figure 14(b)). The electric dipole generates quasi vertically polarized waves (i.e., $E_{\theta)}$ and the horizontally polarized loop generates quasi horizontally polarized waves (i.e., E_ϕ),

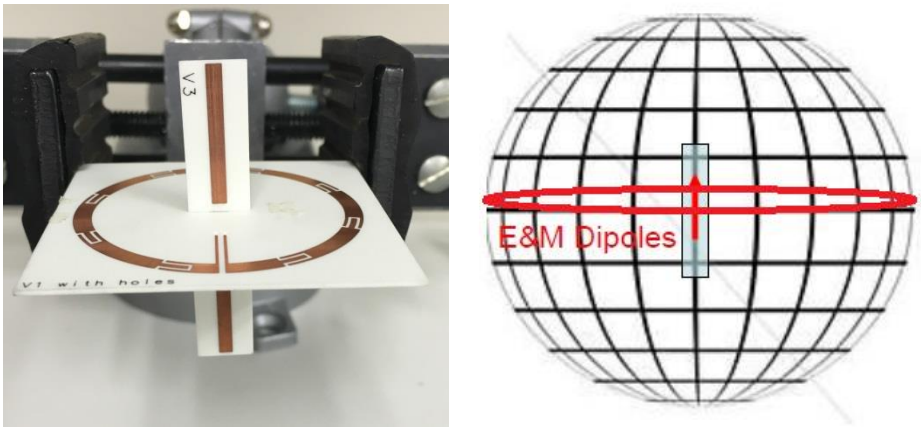

(a) (b)

Figure 14: E&M dipole configuration (a) Collocated arrangement (b) Electric field lines due to collinear arrangement of E&M dipoles

5.3 Simulation Results and Case Studies

Based on the previous discussion, the E&M dipole which is collocated and assembled into a single unit can potentially serve as dual polarized radiating element for Phased Array Radars (PAR). The antennas are aligned in such a manner that they share the same phase center and achieve optimal beam-matching for the two polarization directions. The E&M dipoles are arranged as shown in Figure 15(a) where electric dipole's axis is along z axis and the loop is in XY-plane.

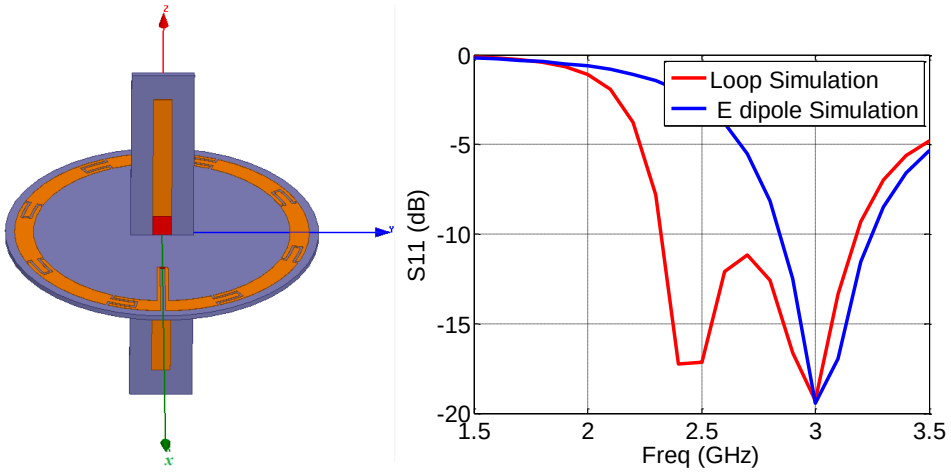

(a) (b)

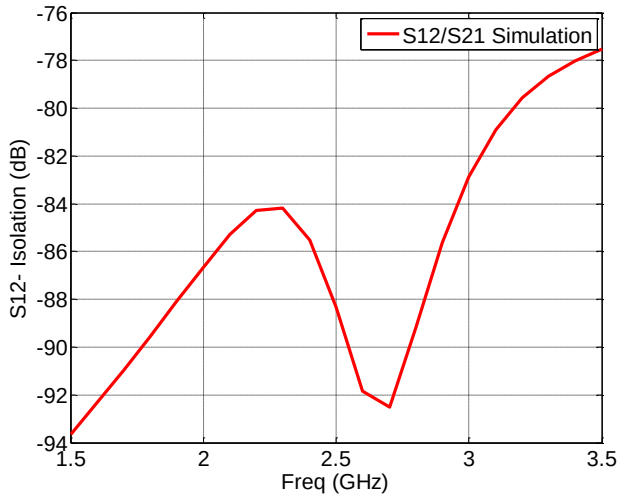

(c)

Figure 15: HFSS design and S-parameters of the collocated EM dipole radiating Element (a) HFSS design (b) Return loss S_{11} (dB) (c) Isolation S_{12}/ S_{21} (dB)

We then focus on the radiation patterns and the principle plane cuts for the radiating elements. There are three different cases of element excitations, which are shown in the following Figures 16-18:

Case1: E & M Dipole Excited Simultaneously:

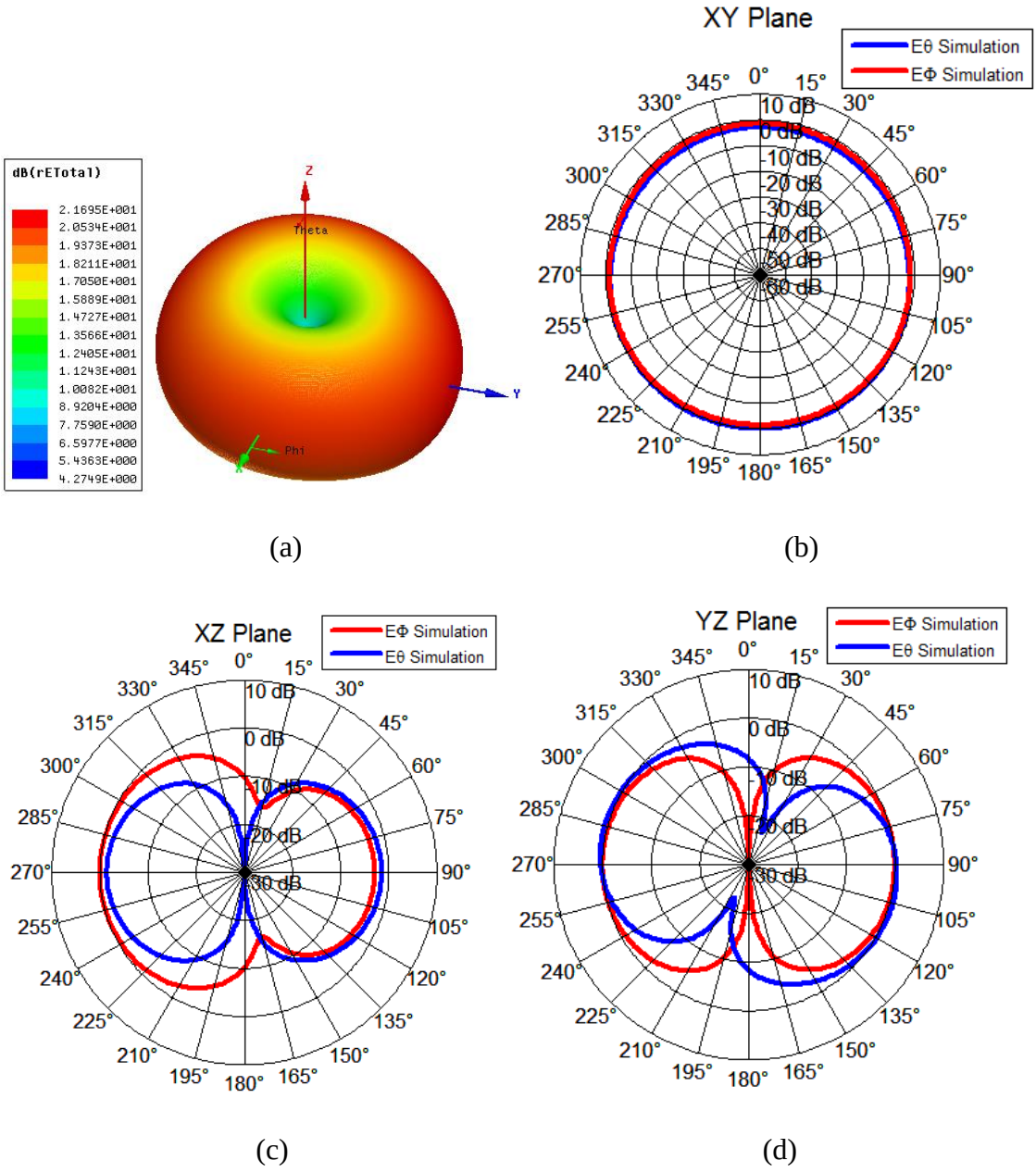

Figure 16: HFSS simulation results when both E&M dipoles are excited simultaneously (a)3-D radiation pattern (b) XY plane cut of the radiation pattern (c) XZ plane cut of the radiation pattern (d) YZ plane cut of the radiation pattern

Case2: Loop (Magnetic) Dipole Excited, E dipole Terminated:

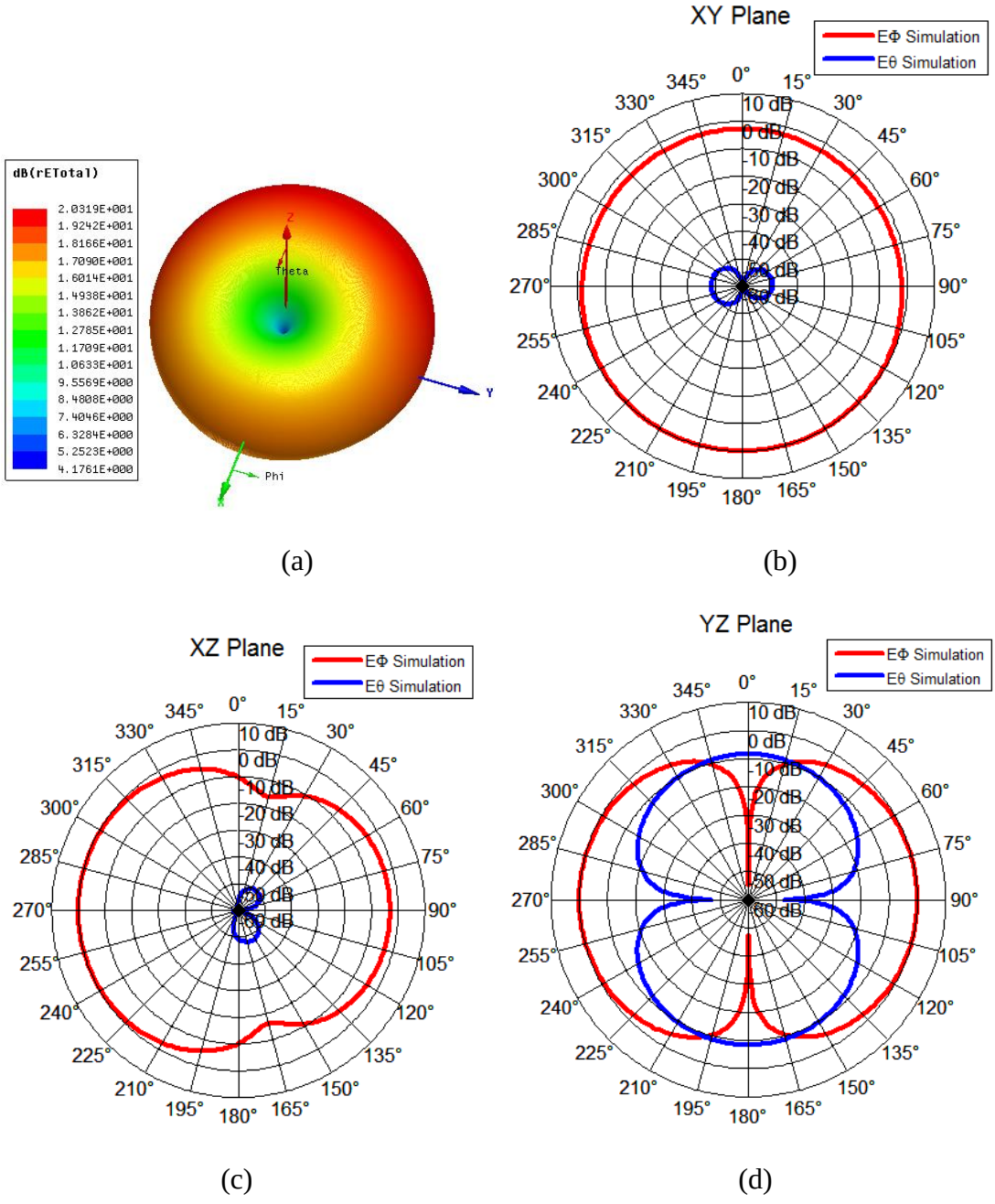

Figure 17: Simulation results when the loop is excited and E-dipole is terminated (a) 3-D radiation pattern (b) XY plane cut of the radiation pattern (c) XZ plane cut of the radiation pattern (d) YZ plane cut of the radiation pattern

Case3: Loop (Magnetic) Dipole Terminated, E dipole Excited:

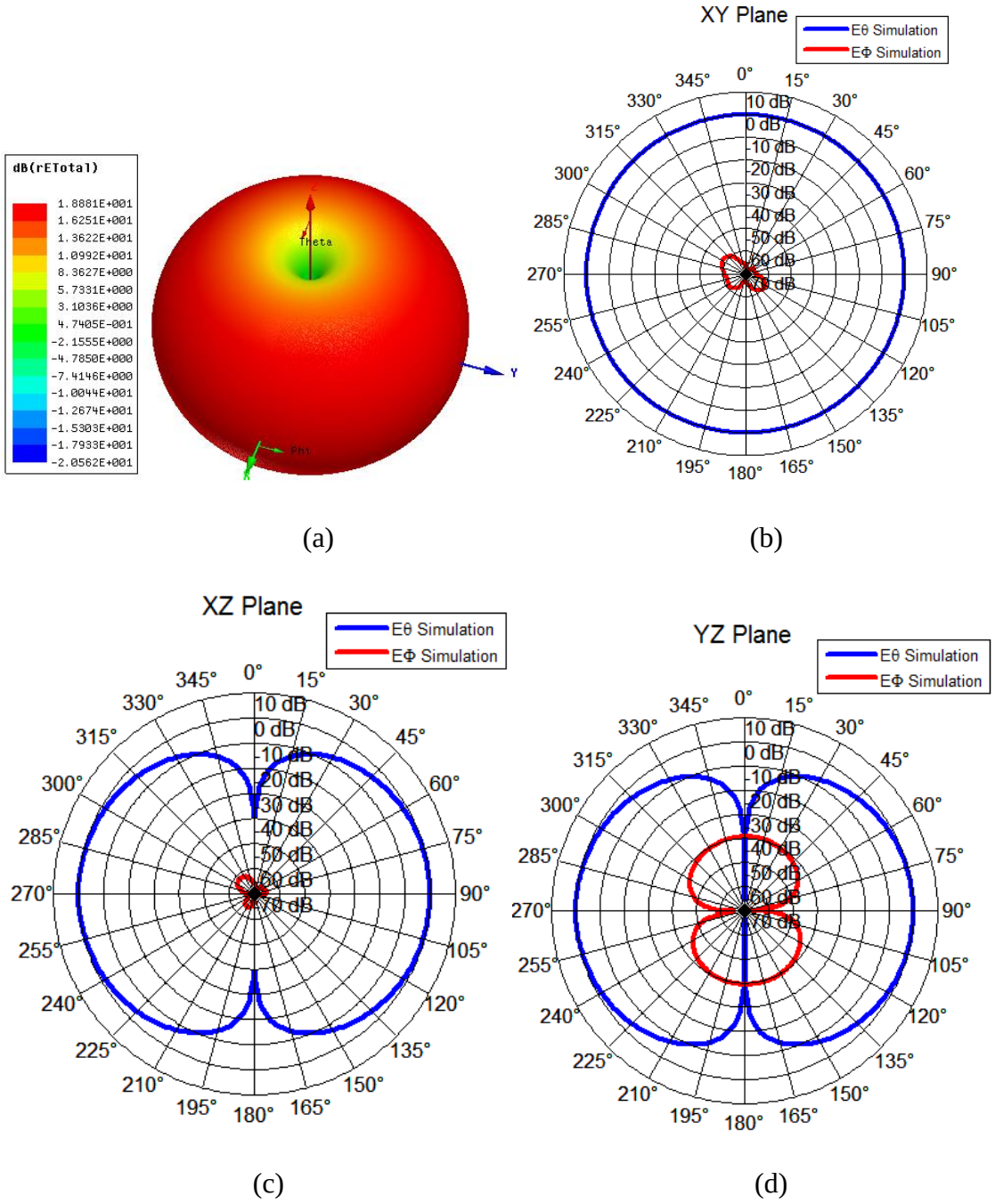

Figure 18: Simulation results when loop is terminated and E Dipole is excited (a) 3-D radiation pattern (b) XY plane cut of the radiation pattern (c) XZ plane cut of the radiation pattern (d) YZ plane cut of the radiation pattern

5.4 Inferences from Simulation Results

The simulation results discussed in Section 5.3 show the S-parameters and different radiation patterns when each of the elements is excited. The return loss (S_{11}) shows both antennas are resonating at 3 GHz. However, all the radiation patterns are plotted at 2.8 GHz because the measurement results have slight shift for these antennas (which will be discussed in Chapter 7 and also seen in Figure 12(a)). Therefore, to facilitate the comparisons of simulation and measurements, all the radiation plots are plotted at 2.8 GHz. The Figure 15(c) shows the port to port isolation between loop and E dipole. The isolation is better than 80 dB in the impedance bandwidth which means there is almost no port leakage of power from the magnetic loop to the E dipole.

It can observed from the case 1in which both E&M dipoles are excited simultaneously, that the horizontally polarized electric field (E_ϕ) produced by magnetic dipole (loop) and the vertically polarized electric field (E_θ) produced by electric dipole are orthogonal and they match very closely, especially in XY plane (which is to be considered as broadside for antenna array). This is because both the antennas radiate fields similar to doughnut shape as illustrated in Figure 17(a) and Figure 18(a). Additionally, the radiation in XZ plane (Figure 16(c)) shows that the magnetic dipole component E_ϕ has slightly more magnitude (in dB) and this can also be seen in XY plane if carefully observed. This asymmetricity might be due to the feed line which radiates more power from the side of the loop where feed line is located.

The case 2 and case 3 shows the radiations patterns when only one of the elements is excited from the collocated EM dipole unit. These radiation patterns are more realistic simulation results for a dual-polarized radiating element for a phased

array radar, because the mutual coupling and the interaction between two antennas elements are taken into consideration in the simulation environment when analyzing these two antennas together as a single radiating element. The cross-polar field (E_θ) for loop is almost about more than 40 dB lower than its co-polar field (E_ϕ). Similarly, the cross-polar field (E_ϕ) for E dipole is almost about more than 50 dB lower than its co-polar field (E_θ). Hence, it can be said that these antennas act as dual to each other and the theory discussed in section 5.1 can be realized practically. The measurement results in anechoic chamber will be discussed in Chapter 7.

Chapter 6: Anechoic Chamber and Procedures

The Anechoic Chambers at Radar Innovation Lab (RIL) at University of Oklahoma is a state of art designed to measure the antenna elements and arrays. These chambers have a controlled environment, all weather capability to perform measurements. The electromagnetic radiation and interference from other sources are minimized by using the high quality RF absorbing material used for covering chamber walls. Among two anechoic chambers at RIL, the small chamber is used for measuring the antennas in this thesis.

6.1 Near-field Antenna Range and Anechoic Chamber at RIL

The small anechoic chamber is generally used to measure near-field data which consists of amplitude and phase distributions by using a scanning field probe over a planar, cylindrical or spherical co-ordinate system. The OU's small anechoic chamber is manufactured by Nearfield Systems Inc. (NSI). The co-ordinate system of the chamber can be seen in the Figure 19. The scanning probe can move along two tracks (X and Y) and also rotates horizontally and vertically. These probes are interchangeable rectangular waveguides and each has its specific frequency band of operation.

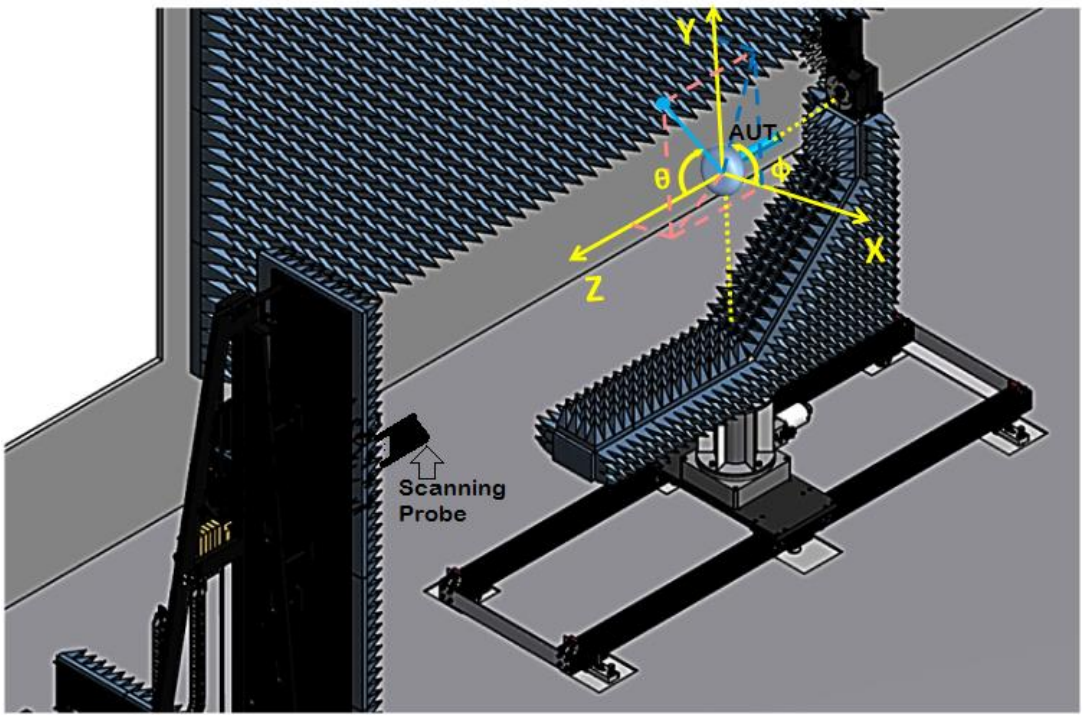

Figure 19: Near field chamber co-ordinate system

The L shaped positioner is used to mount the antennas and rotate in two degrees of freedom i.e. in Azimuth (ϕ) and Elevation (θ). All the cables from the antenna go through the bulkhead of the positioner and then connected outside to the Agilent PNA Network Analyzer (10 MHz to 50 GHz). The movement of the scanning probe and the positioner are controlled by high precision servo motors manufactured by NSI (NSI 5912 Intelligent Measurement Controller and NSI 5913 Antenna Range Controller). All the scanned data is displayed on a desktop computer by means of the NSI Graphical User Interface Application.

If observed carefully, the axes configuration for the OU's chamber has a different configuration as compared to standard co-ordinate system used in theory and also in weather radar applications. This is illustrated in the Figure 20.

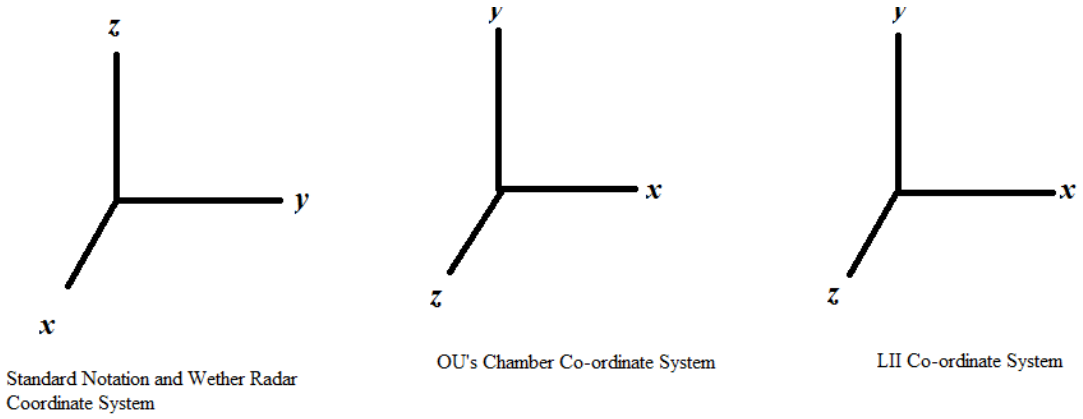

Figure 20: Comparison of different co-ordinate systems

In common practice, center axis of the antenna is directed towards polar axis of the radiation sphere. For example: An Electric Dipole's axis should be along the z axis (which is the horizontal plane defined in the chamber) and the main beam is along x axis (i.e., the roll axis is to be in the aperture plane of the AUT). If this said antenna configuration is followed and measurements are carried out in a manner such that the far-field wave guide probe is said to receive horizontally polarized radiation then, the measured pattern over 360 degrees of rotation will give the co-polar or E_θ field (for an electric dipole). If this measurement is repeated for another 360 degrees and this time the source probe is rotated by 90 degrees about the initial position, then the measured pattern will be cross-polar or E_ϕ field (for an electric dipole). This E_θ and E_ϕ measurements match the spherical co-ordinates used by weather radar engineers and there is no need to apply any forms of transformations. This said straight forward procedure is followed in this thesis to avoid any confusion and ambiguity related to axis transformation, and the results are displayed in Chapter 7.

6.2 Setup Procedure

Before starting the actual measurement process, a setup needs to be performed which is shown below.

1. Check the operating frequency of the AUT and select the appropriate scanning waveguide probe.
2. Select the appropriate antenna analysis co-ordinate system (planar, cylindrical or spherical) and based on the selection, connect the wire to activate the correct co-ordinate system
3. Depending on the type of antenna or array (AUT), attach it to the positioner with the help of mounting structures (if any) for spherical and cylindrical system. For planar scanning just put the AUT in front of the scanning probe
4. If far-field measurements are needed to be performed, the distance between the scanning probe and the AUT must be more than 5λ. If near-field measurements are to be performed then maintain a distance of less than 3λ.
5. Index the motors and position of the scanner
6. Terminate all the ports which are not excited
7. Make sure the AUT and scanning probe are aligned in a straight line. A laser can be used for this purpose

8. Now define the range of frequencies over which the antenna is to be measured. This can be done by entering start and stop frequencies. Click generate frequency list and load suggested dwells. This sends command to PNA to receive the data over these frequencies.

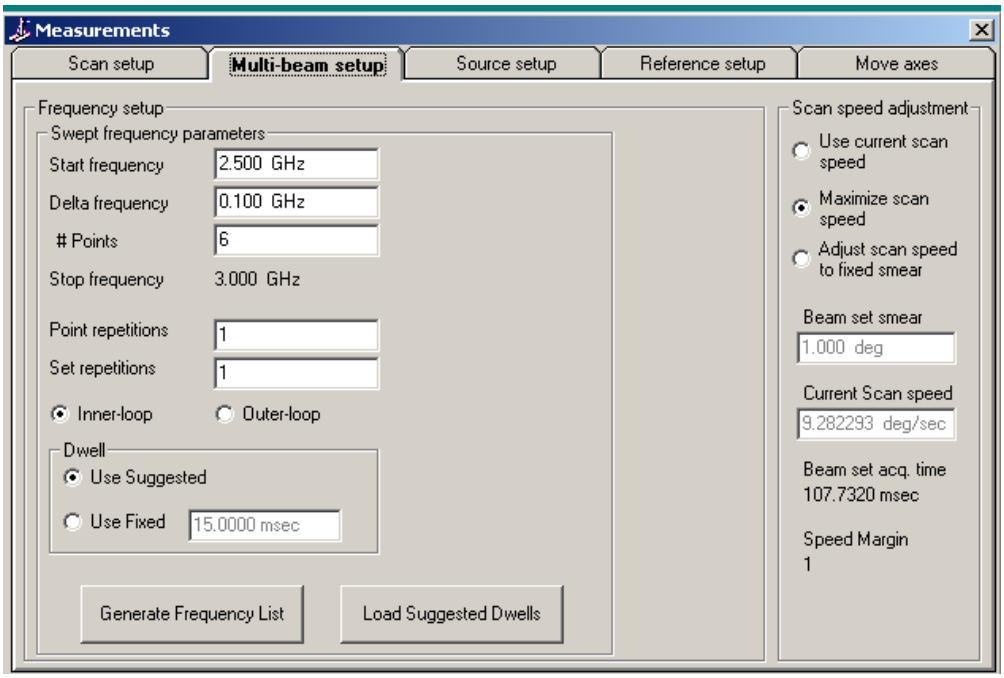

Figure 21: Selecting the frequencies

9. Now under the scan setup menu define the values for measuring distance which is the distance from scanning probe to AUT. MRE is the size of AUT. Define the scanning range for azimuth (ϕ) and elevation (θ) and select the appropriate scan axis.

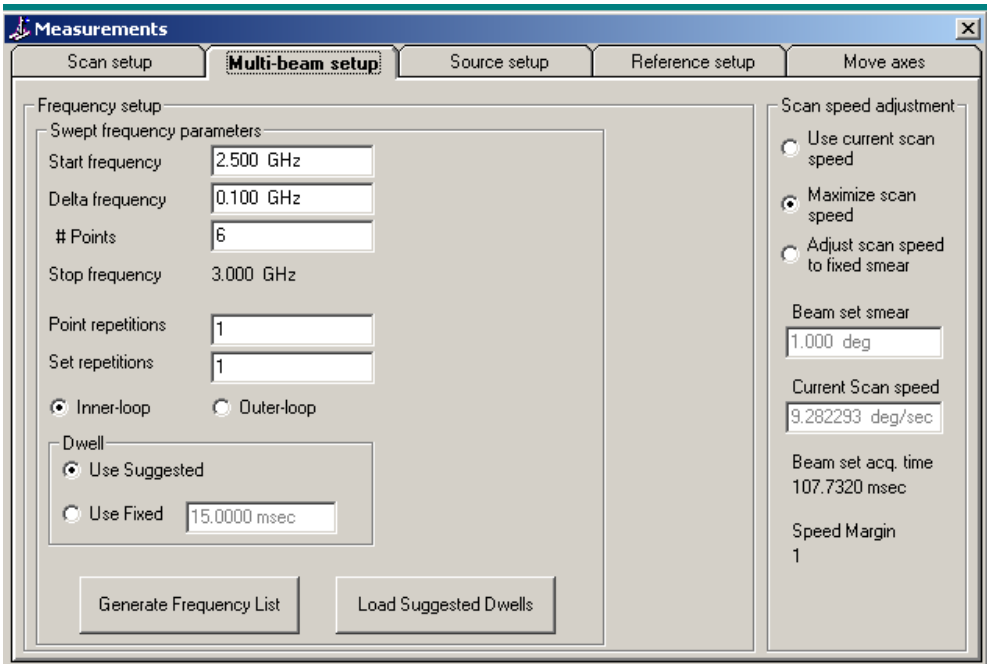

Figure 22: Scan setup

10. Start the measurement by clicking acquire option.
11. After the measurements are complete, the far field display gives the options to plot the data over different angles. As mentioned in the earlier section, we are measuring E_θ and E_ϕ which is nothing but co and cross pol. So L2 Eth-Ephi is same.

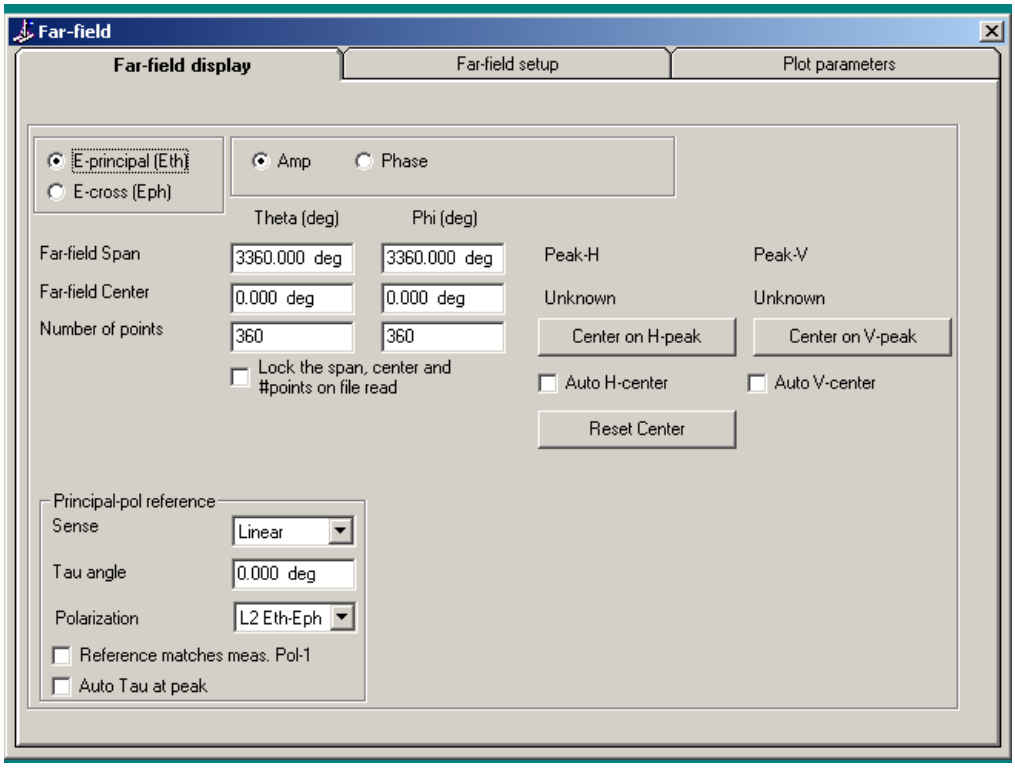

Figure 23: Far-field display setup

12. Plot the data and extract it in csv format to plot in Matlab.
13. To finish the measurement process, abort the application and remove the AUT setup.

Chapter 7: Anechoic Chamber Measurement Results of E&M Dipoles

7.1 Loop Antenna as Magnetic Dipole

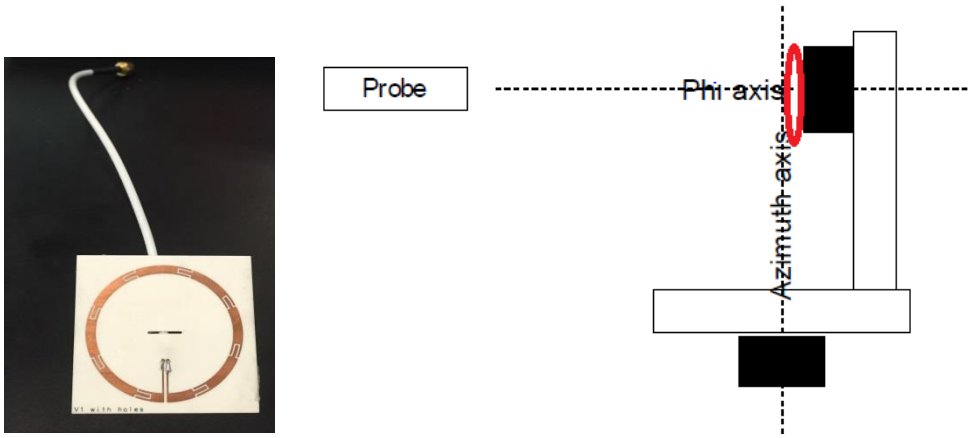

Figure 24: Fabricated magnetic dipole antenna and the measurement configuration in NF Chamber (AUT is aligned to point null at the source probe)

The fabricated loop antenna is measured with the help of the mounting structure such that loop lies in the XY plane and pointing null towards the scanning probe. The results shown below are at 2.8 GHz.

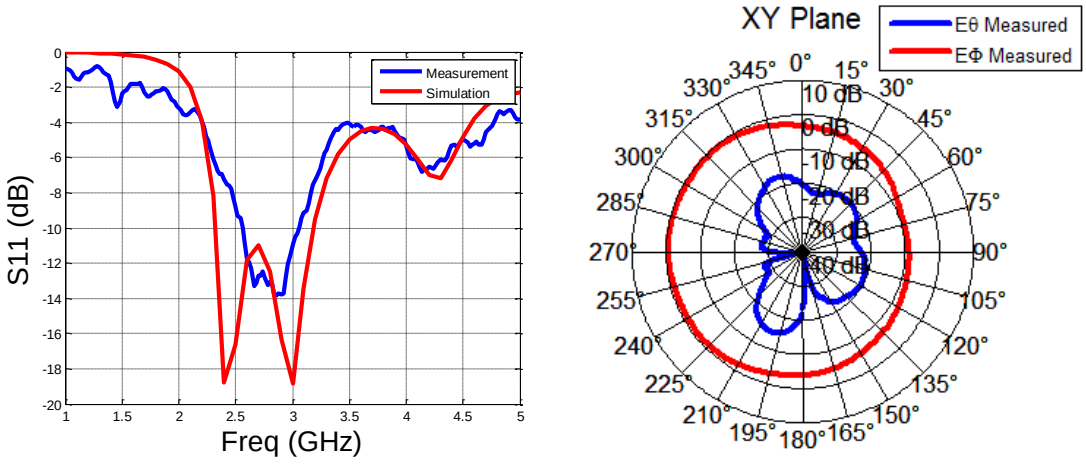

(a) (b)

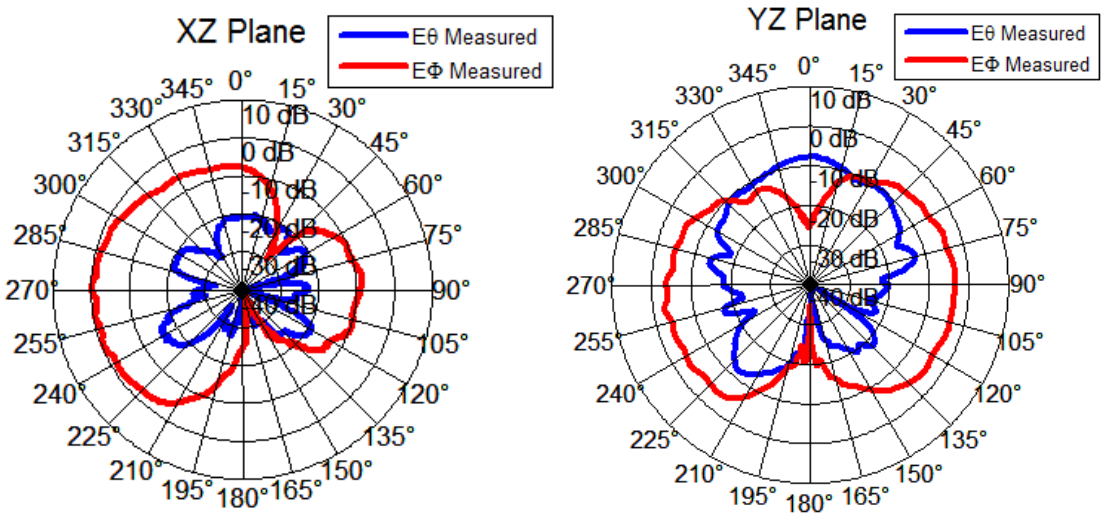

(c) (d)

Figure 25: Measurement results for the loop antenna(a) S_{11}(dB) Return Loss (b) XY plane cut of the radiation pattern (c) XZ plane cut of the radiation pattern (d) YZ plane cut of the radiation pattern

7.2 Printed Electric Dipole Antenna

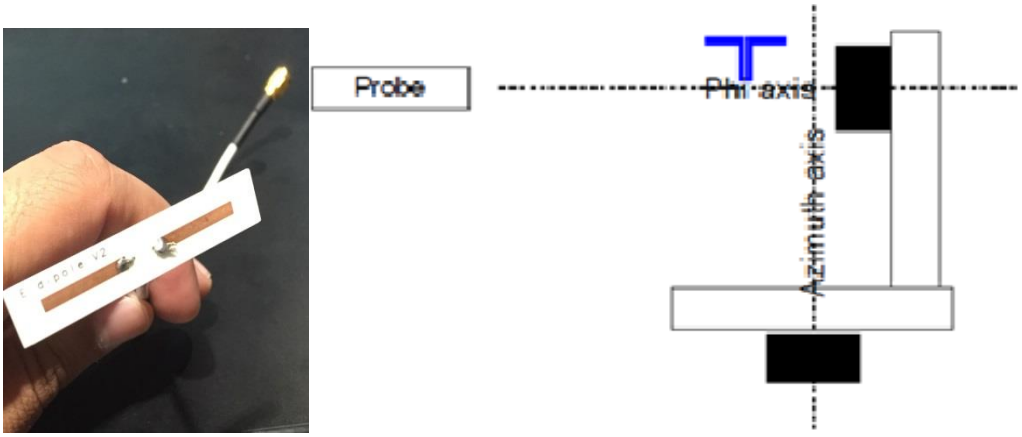

Figure 26: Fabricated Electric dipole antenna and measurement configuration in the NF Chamber (E dipole is aligned along Z axis)

The fabricated loop antenna is measured with the help of the mounting structure such that electric dipole's axis is along the Z-axis of the chamber and pointing null towards the scanning probe. The results shown below are at 2.8 GHz.

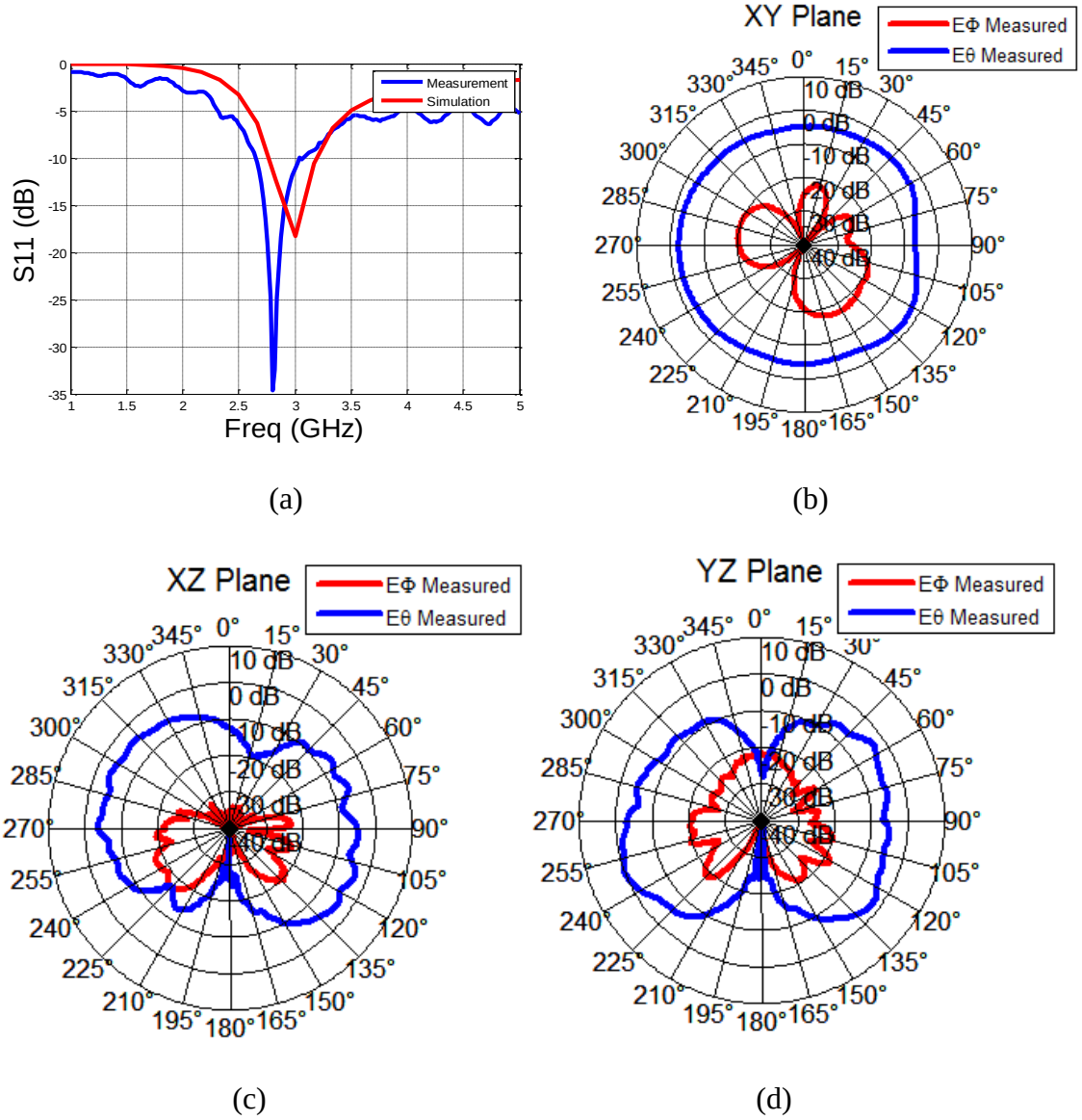

Figure 27: Measurement results for printed electric dipole antenna (a) S_{11}(dB) Return Loss (b) XY plane cut of the radiation pattern (c) XZ plane cut of the radiation pattern (d) YZ plane cut of the radiation pattern

7.3 Loop Antenna and Electric Dipole Antenna Excited Simultaneously

Figure 28: Fabricated E&M Collocated Dipole Antenna and its configuration in NF Chamber (E dipole is aligned along Z axis and Loop is aligned to point Null at the source probe)

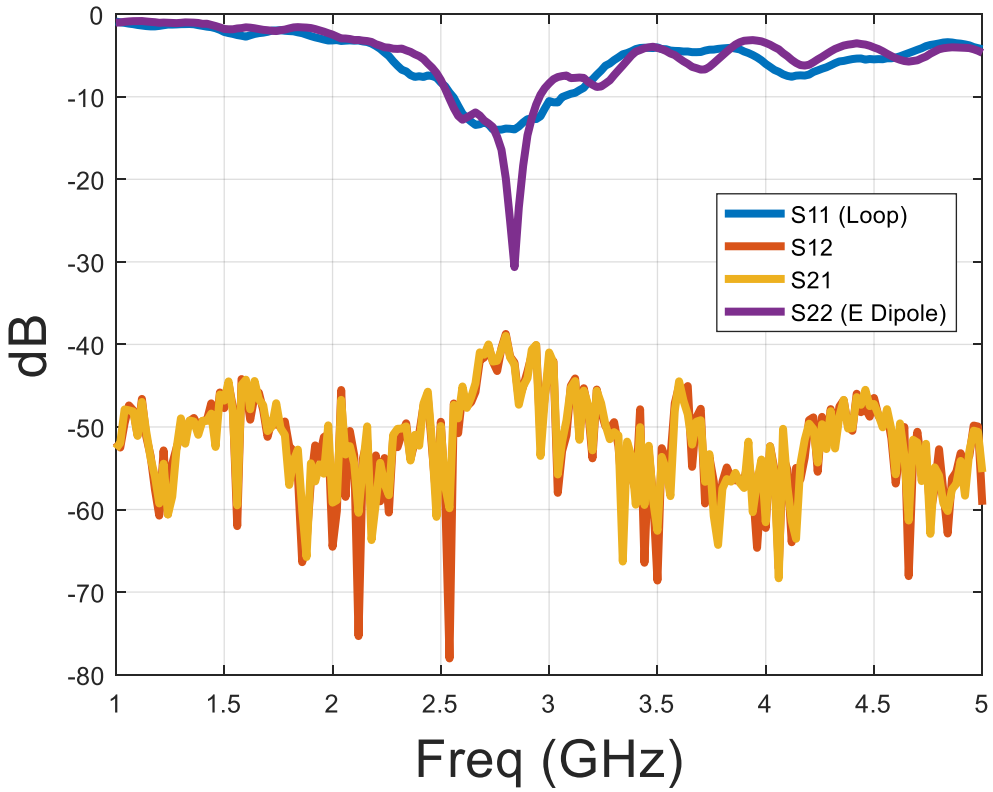

(a)

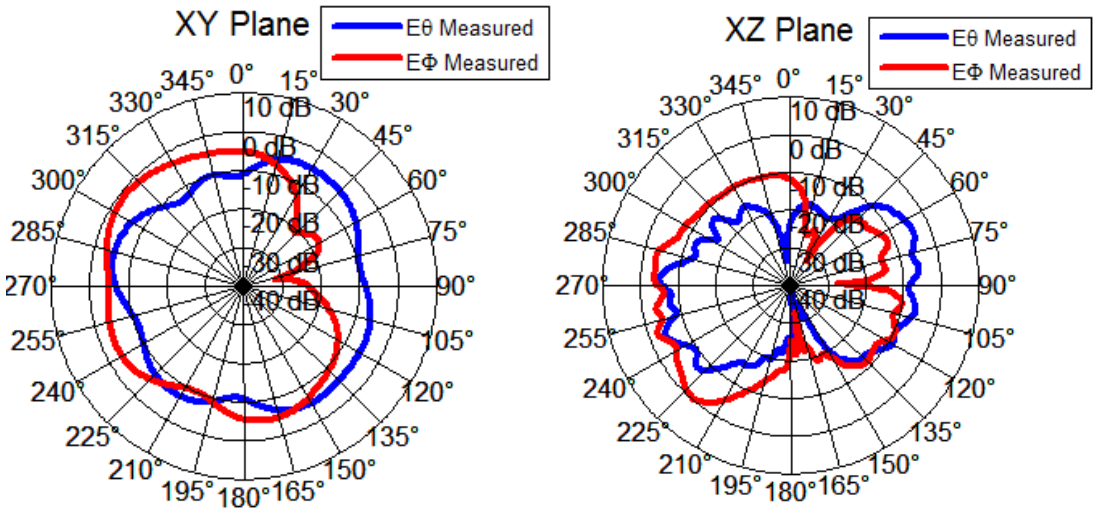

(b)

(c)

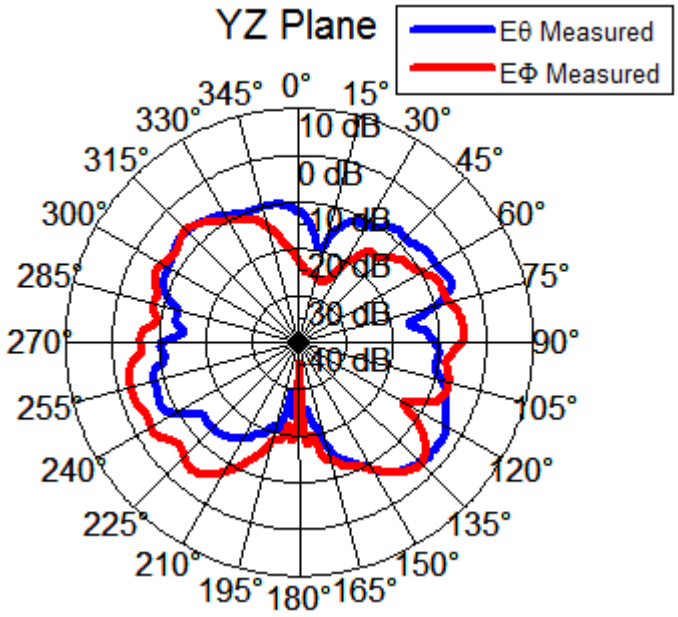

(d)

Figure 29: Measurement results when the loop antenna and E dipole antenna are excited simultaneously (a) Measured S-parameters (dB) (b) XY plane cut of the radiation pattern (c) XZ plane cut of the radiation pattern (d) YZ plane cut of the radiation pattern

7.4 Comparison of the Proposed Loop Antenna and Commercial Magnetic Dipole

This section shows a comparison of proposed fabricated loop with commercially available Magnetic dipole. The commercial magnetic dipole is manufactured by SATIMO and the comparisons are made at 2.8 GHz.

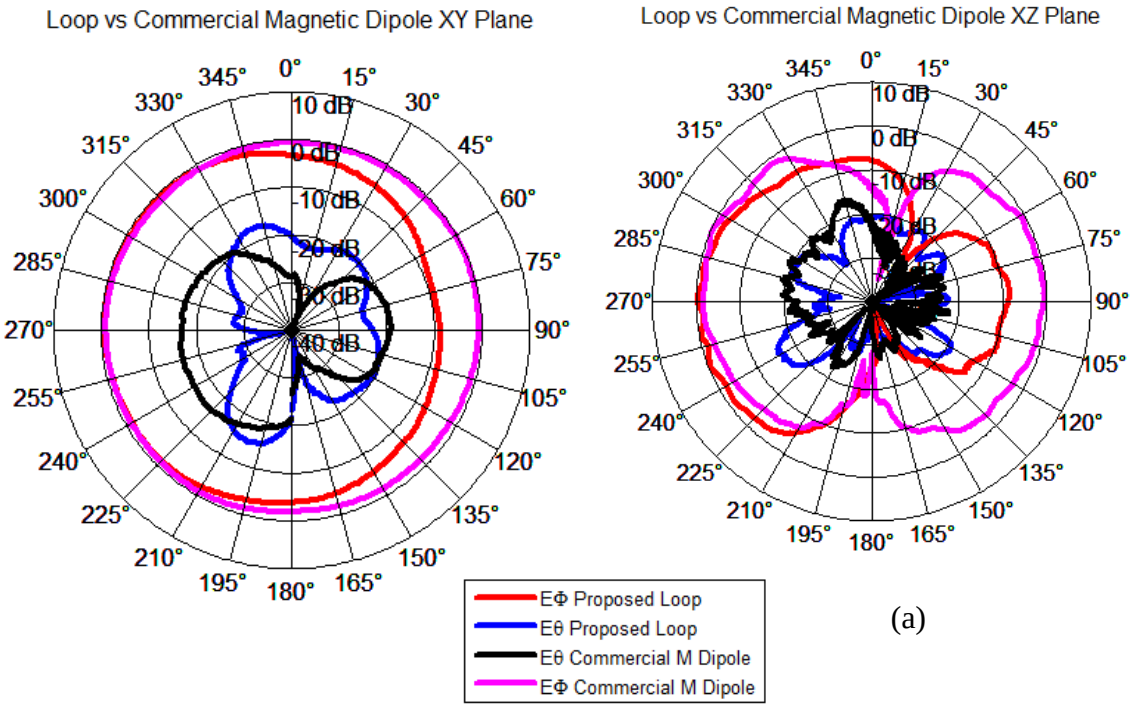

(a)

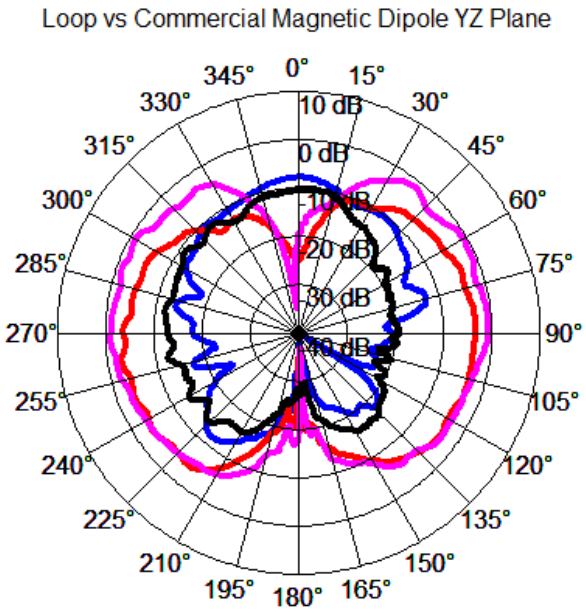

(c)

Figure 30: Comparison of proposed loop vs commercial magnetic dipole (a) XY plane cut of the radiation pattern (b) XZ plane cut of the radiation pattern (c) YZ plane cut of the radiation pattern

7.5 Comparison of the Proposed Electric Dipole Antenna and Commercial Electric Dipole Antenna

This section shows a comparison of proposed printed Electric Dipole with commercially available Electric Sleeve dipole. The commercial Electric dipole is manufactured by SATIMO and the comparisons are made at 2.8 GHz.

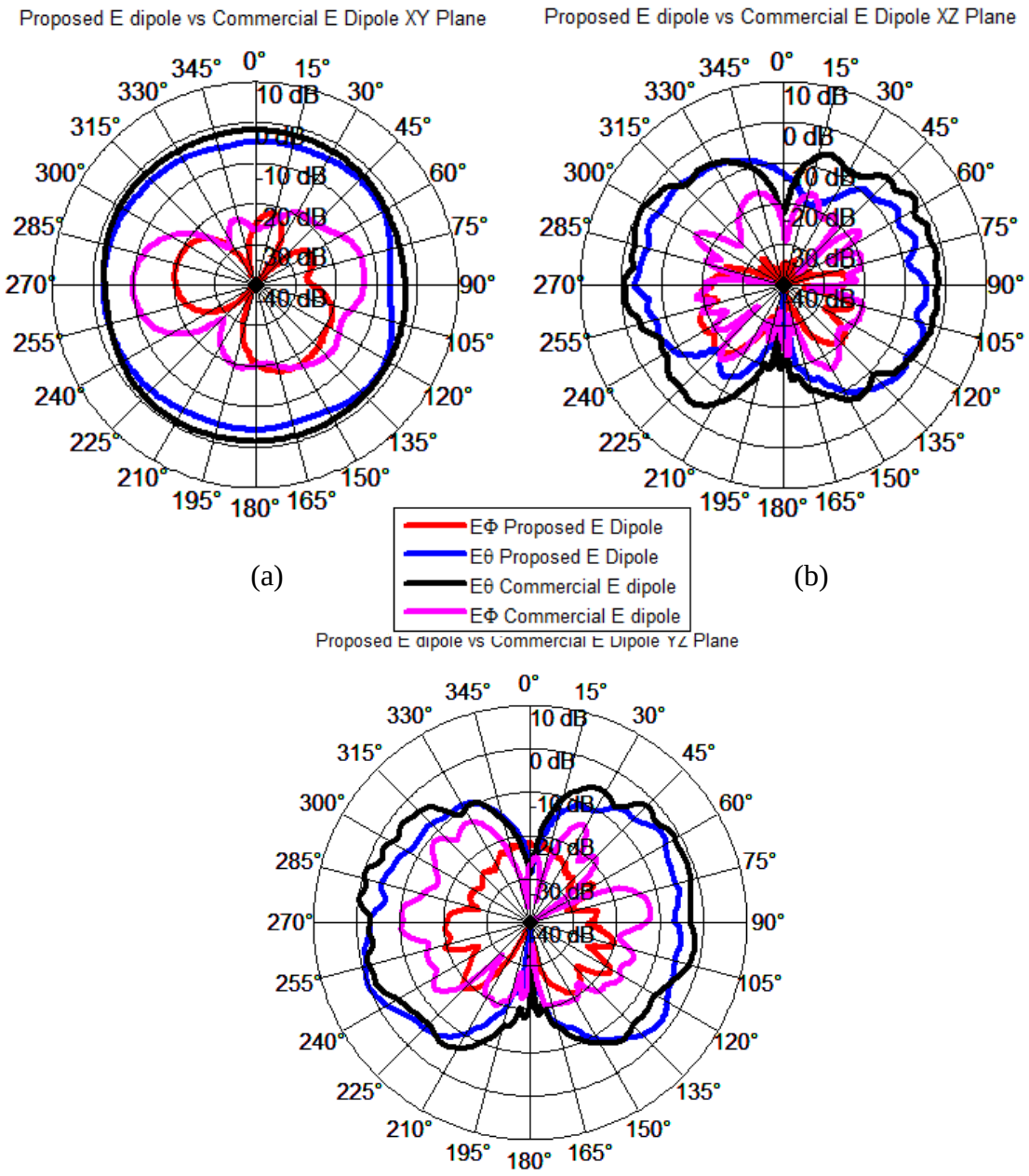

Figure 31: Comparison of proposed E dipole vs commercial E dipole (a) XY plane cut of the radiation pattern (b) XZ plane cut of the radiation pattern (c) YZ plane cut of the radiation pattern

7.6 Conclusions from the Measurement Results

According to the design discussed in Chapter 3, Chapter 4 and Chapter 5, the prototypes of the proposed antennas were fabricated and measured. The measurement procedure was followed the way it was discussed in the Chapter 6.

Section 7.1 shows the radiation characteristics of fabricated loop. The impedance bandwidth of the measured antenna is about 500 MHz, which is slightly less than the simulation result. The radiation patterns in the principal planes can be seen in Figure 25. The horizontally polarized loop radiates the electric fields in ϕ and θ direction which corresponds to co-polarization (E_ϕ) and cross-polarization (E_θ) patterns respectively. The cross polarization is 20 dB lower than the co-polar peak. The XY plane is of the loop should be given considerable attention as this will be the plane of radiation when the loop is going to be used for construction of an array. It can be observed that the radiation fields of the loop are close to an ideal magnetic dipole as it exhibits a pattern similar to that of a figure eight with a null along its axis (in elevation plane) and has maximum radiation along the plane of the loop (XY-plane). The asymmetricity of XZ plane can be seen and this might be due the radiation from the feed line. It is because of the same reason that the Omni-directionality of the loop is slightly distorted in XY plane.

The measurement results of the printed electric dipole shown in section 7.2 are at 2.8 GHz which is the same operating frequency to that of loop. The electric dipole proposed here has about 400 MHz bandwidth. Since the electric dipole is vertically polarized, it radiates electric fields in θ and ϕ direction which corresponds to co-polarization (E_θ) and cross-polarization (E_ϕ) patterns respectively. The cross

polarization measured is 20 dB for the XY plane which is again the plane of radiation when for array design.

Next, the section 7.3 illustrates when both of these antennas are excited together, the radiation patterns in most of the planes match approximately to each other and act as a dual antennas to themselves. The Figure 29 shows the S parameters and the radiation patterns in the principal planes. Both of the antennas are excited at 2.8 GHz and the isolation between the ports is almost 40 dB in the impedance bandwidth. As discussed in section 5.1 of Chapter 5, these elements have maximum along XY plane and the electric field of electric dipole (E_θ) is orthogonal to the electric field of the loop (E_ϕ) everywhere. These radiation patterns have a good agreement with the HFSS simulation results shown in Figure 16, however the cross polarization level is higher. This is because the HFSS simulation uses an ideal feed whereas in practical realization we have feed lines and twin lead cables soldered to the antenna.

The performances of the proposed antennas can also be compared with the commercially available EM dipole antenna available in the industry. The pair which is used here is manufactured by SATIMO/MVG and used predominantly in many applications in the industry for gain reference, efficiency reference and chamber reflectivity evaluation [26]. The co-pol and cross-pol comparisons can be seen in section 7.4 and section 7.5. The Table 6 shows a brief comparison of the specifications.

Specification	**Proposed E&M Dipole**	**Commercial E&M Dipole**
Cross-pol Level	About 20 dB in all planes	About 15-20 dB in all planes

Form	Microstrip Planar Form	Linear Wire (3D structure)
Feed	Twin-lead Feed	Coaxial Feed SMA
Bandwidth	500 MHz (Loop) 400 MHz (E Dipole)	200 MHz (Magnetic dipole) 700 MHz (E Dipole)
Cost	$45 per unit	$2,000 per unit
Weight	10 grams each	About 200 grams each
Use for Array	Yes. Both E&M dipoles can be used as a single dual polarized element for arrays	No. Each dipole unit is separate and does not facilitate building an array.
Robustness	Delicate	Rigid

Table 6: Comparison between proposed E&M dipoles and commercial E&M dipoles

Chapter 8: E&M Dipole Array

Based on the design of the proposed E&M Dipole antennas, an array can be constructed with these elements collocated in a single unit to emulate a linear subarray for future MPAR (Multi-functional Phased Array Radar). This Chapter shows the initial layout for such an array and simulation results based on HFSS.

8.1 Array Design and Simulation using HFSS

An array can be constructed by spacing each of the collocated E&M dipole unit half wavelengths apart ($\frac{\lambda}{2}$). An investigation of using these elements in a linear form of array is being carried out. The Figure 32 shows a simple arrangement of such 8 collocated E&M Dipole units.

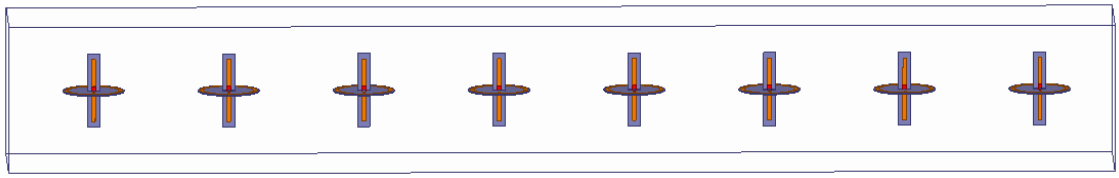

Figure 32: A simple 8 element E&M dipole array in HFSS

If each of these 8 collocated units (16 elements) are excited with equal phase and equal amplitude, then it can be seen in Figure 33(a) that co-polar H and V fields match exactly to each other which meets the requirement for weather applications (proves to be effective in extracting more hydrological parameters) and gives better resolution of the target [2]. On the other hand, if only magnetic loop is transmitting and E dipole is receiving or vice versa, the cross-polar radiation is observed to be more than 70 dB lower than the peak co-polar field. These results are illustrated in Figure 33.

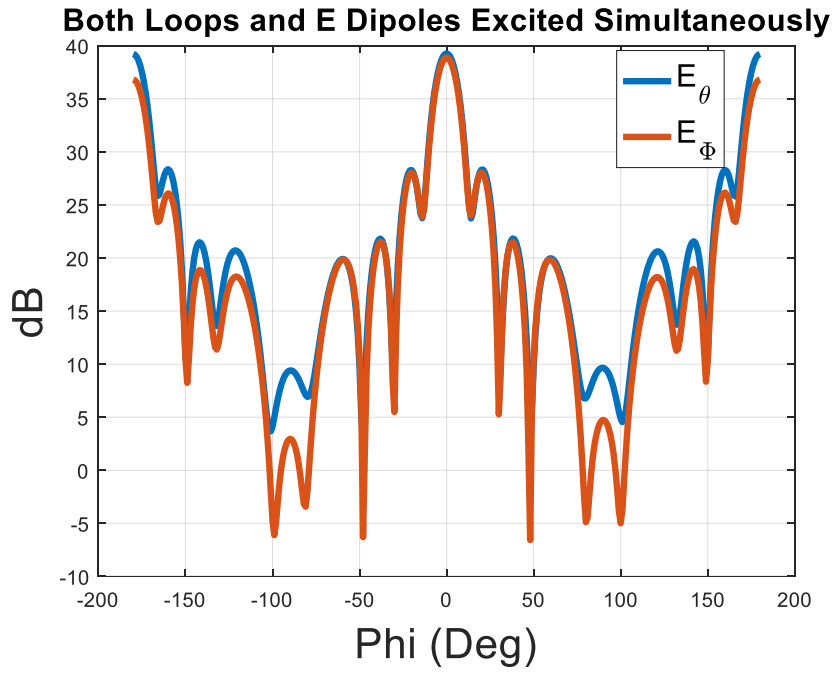
Both Loops and E Dipoles Excited Simultaneously
dB
Phi (Deg)
E θ
E Φ
40
35
30
25
20
15
10
5
0
-5
-10
-200
-150
-100
-50
0
50
100
150
200

(a)

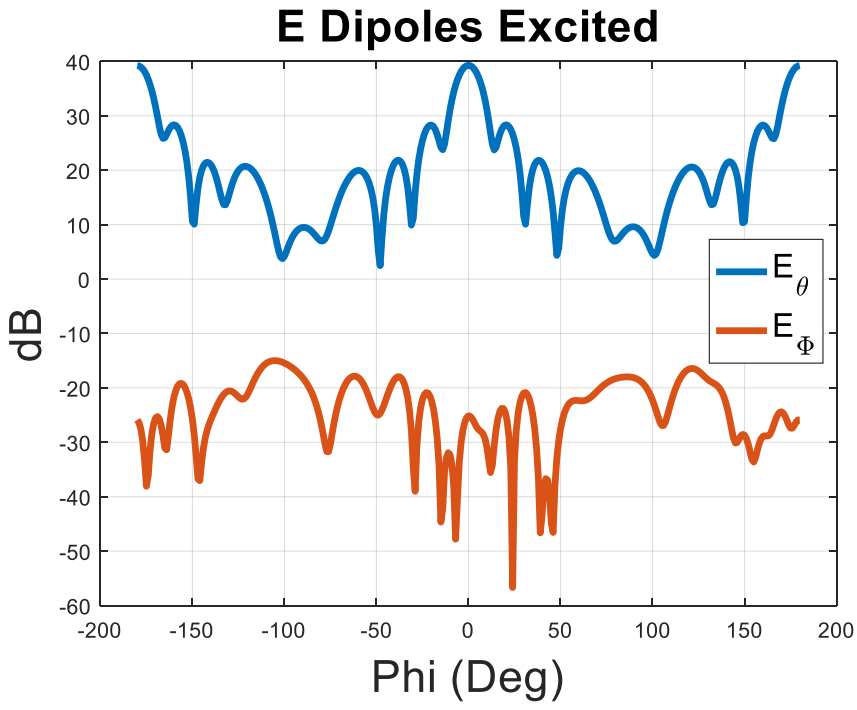
E Dipoles Excited
dB
Phi (Deg)
E θ
E Φ
40
30
20
10
0
-10
-20
-30
-40
-50
-60
-200
-150
-100
-50
0
50
100
150
200

(b)

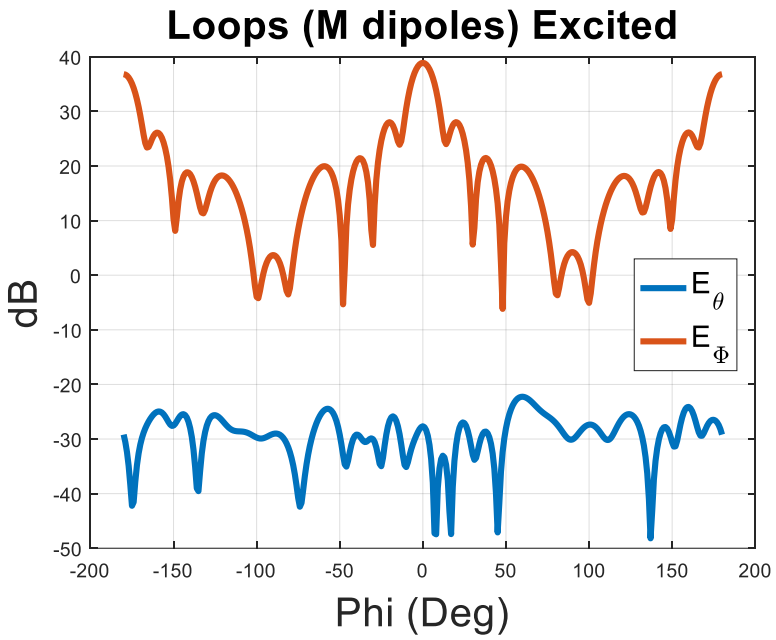

(c)

Figure 33: Illustration of co-polar and cross-polar fields (amplitudes in dB) (a) when both E&M elements are excited (b) Only the magnetic loops are excited (c) Only the electric dipoles are excited

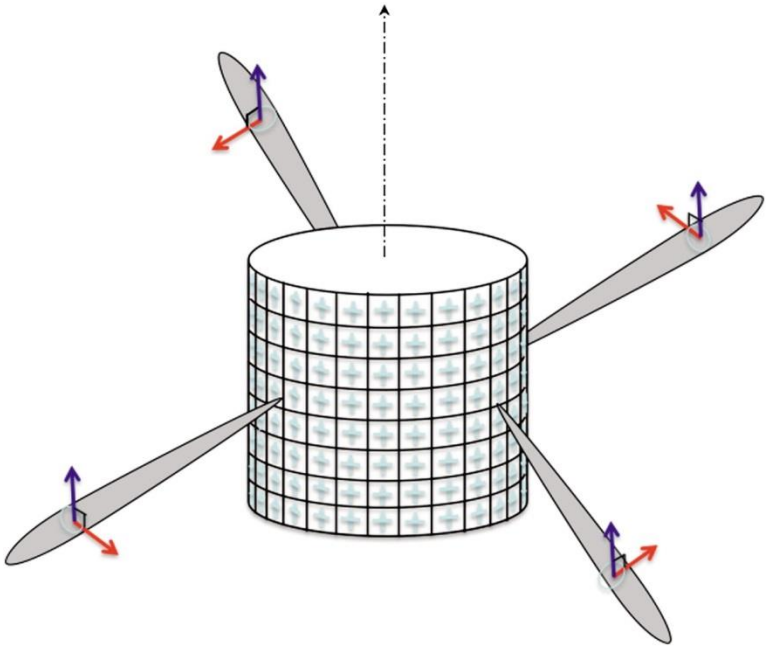

Figure 34: CPPAR with a pair of dipoles for each array element.[8]

It should be noted that these simulation results shown in Figure 32 and Figure 33 is based on ideal assumptions in simulation environment. However in the practical realization of the array, we need to consider the radiation from the feed lines, imperfections in fabrications, support structures and backplane (or aluminum plate) for the purpose of support structure for the array and also for the electronics. This can actually have an adverse effect on the cross polarization levels of the array.

The concept of E&M dipole can be used not only in linear arrays, but also for implementing a cylindrical polarimetric phased array radar (CPPAR) as illustrated in Figure 34 . The use of cylindrical array has advantages like scan invariant polarization basis and low sensitivity loss [8]. In addition to this, the use of the dipole elements can avoid surface waves and creeping waves. However, this is at the cost of more complex and expensive fabrication process.Initial array fabrication and testing is to be performed in a larger array testbed called Configurable Phased Array Demonstrator (CPAD) at the Radar Innovations Laboratory (RIL), University of Oklahoma.

Chapter 9: Conclusions

A dual polarized radiating element for MPAR is proposed by using two simple types of microstrip radiating elements. As aforementioned, this thesis is a step towards designing and realizing a dual-polarized array element based on electromagnetic dipoles concept. The intention of this thesis is to demonstrate a possible new design and building a foundation on which future research can be conducted.

This thesis implements and investigates the concept of using a collocated electric and magnetic dipole for Phased Array Radars. The array element is a fundamental building block for an array antenna and it is required that these elements have high cross polarization suppression capacity. The magnetic dipole is realized by a simple loop with capacitive loading which maintains uniform surface current. The electric dipole takes the form of printed dipole. An ideal electric dipole should produce only vertically polarized waves (i.e., E_θ) whereas an ideal magnetic dipole should generate only horizontally polarized waves (i.e., E_ϕ) which is free of any cross-polar radiation. Nevertheless, these elements when realized practically have secondary cross-polar fields due to the design of the feed lines, radiation from feed lines, practical factors in design and assembly. For weather polarimetry it is expected that the elements maintain cross polarization factor of about 40 dB for simultaneous transmit/receive and 20 dB for alternate transmit/receive [6]. However, these figures are for the array level design but we expect that if the cross polarization isolation is minimized at the element level, then it is expected that will array level implementation one can achieve this goal.

The measurements performed in the Anechoic Chambers show the cross-polarization of these elements to be about 20dB lower than peak co-polar field. These elements are also compared with some commercially available dipoles. The measurement process involves extensive measures taken to achieve the best possible results but the interferences from the feed lines and mounting structures are evident. In addition, the limitations such as availability of ideal probes which have purer linear polarization as compared to AUT make the suppression of cross-polarization more difficult.

There are few aspects in which the current design of the elements can be improved. One significant improvement can be design of a proper feed line using techniques such as proximity feed, aperture coupled feed etc. This feeding design can be carried forward and improved by also considering the mechanical design and ease of feeding these elements when assembled into an array. It would be lucrative to see a linear array constructed using these elements such that the cross-polar fields are further reduced.

References

[1] (2016, 20th January 2016). *NOAA NATIONAL SEVERE STORMS LABORATORY* [Online]. Available: http://www.nssl.noaa.gov/tools/radar/mpar/

[2] D. S. Zrnic, V. M. Melnidov, and R. J. Doviak, "Issues and challenges for polarimetric measurement of weather with an agile beam phased array radar," NOAA/NSSL report, [Updated: 2 May 2013]2013.

[3] C. E. Baum, "Symmetry in electromagnetic scattering as a target discriminant," in *Optical Science, Engineering and Instrumentation'97*, 1997, pp. 295-307.

[4] D. Vollbracht, "Understanding and optimizing microstrip patch antenna cross polarization radiation on element level for demanding phased array antennas in weather radar applications," *Advances in Radio Science,* vol. 13, pp. 251-268, 2015.

[5] M. Kuloglu, "Development of a Novel Wideband Horn Antenna Polarizer and Fully Polarimetric Radar Cross Section Measurement Reference Target," The Ohio State University, 2012.

[6] Y. Wang and V. Chandrasekar, "Polarization isolation requirements for linear dual-polarization weather radar in simultaneous transmission mode of operation," *Geoscience and Remote Sensing, IEEE Transactions on,* vol. 44, pp. 2019-2028, 2006.

[7] F. Mastrangeli, G. Valerio, A. Galli, A. De Luca, and M. Teglia, "An attractive S-band dual-pol printed antenna for multifunction phased array radars," in *Antennas and Propagation (EUCAP), Proceedings of the 5th European Conference on,* 2011, pp. 514-516.

[8] G. Zhang, R. J. Doviak, D. S. Zrnic, R. Palmer, L. Lei, and Y. Al-Rashid, "Polarimetric phased-array radar for weather measurement: a planar or cylindrical configuration?," *Journal of Atmospheric and Oceanic Technology,* vol. 28, pp. 63-73, 2011.

[9] C. A. Balanis, *Antenna theory: analysis and design* vol. 1: John Wiley & Sons, 2005.

[10] W. J. Wu, R. Fan, Z. Y. Zhang, W. Zhang, and Q. Zhang, "A shorted dual-polarized cross bowtie dipole antenna for mobile communication Systems," in *General Assembly and Scientific Symposium (URSI GASS), 2014 XXXIth URSI*, 2014, pp. 1-4.

[11] K. M. Mak, H. Wong, and K. M. Luk, "A Shorted Bowtie Patch Antenna With a Cross Dipole for Dual Polarization," *IEEE Antennas and Wireless Propagation Letters,* vol. 6, pp. 126-129, 2007.

[12] Y. Liu, H. Yi, F. W. Wang, and S. X. Gong, "A Novel Miniaturized Broadband Dual-Polarized Dipole Antenna for Base Station," *IEEE Antennas and Wireless Propagation Letters,* vol. 12, pp. 1335-1338, 2013.

[13] A. Ludwig, "The definition of cross polarization," *Antennas and Propagation, IEEE Transactions on,* vol. 21, pp. 116-119, 1973.

[14] D.Acosta. (2016, 23 rd February). *Enriched Physics 2 Lecture* [Web]. Available: http://www.phys.ufl.edu/~acosta/phy2061/lectures/MagneticDipoles.pdf
[15] R. Garg, *Microstrip antenna design handbook*: Artech house, 2001.
[16] J. T. Aberle and D. M. Pozar, "Accurate and Versatile Solutions for Probe–Fed Microstrip Patch Antennas and Arrays," *Electromagnetics,* vol. 11, pp. 1-19, 1991.
[17] R. K. Mirza, Y. R. Zhang, D. Zrnic, and R. Doviak, "Dual-Polarized Radiating Elements Based on Electromagnetic Dipole Concept."
[18] J. D. Kraus, *Antennas*, 1988.
[19] D. Foster, "Loop antennas with uniform current," *Proceedings of the IRE,* vol. 32, pp. 603-607, 1944.
[20] R. Li, N. Bushyager, J. Laskar, and M. Tentzeris, "Circular loop antennas reactively loaded for a uniform traveling-wave current distribution," in *Antennas and Propagation Society International Symposium, 2005 IEEE*, 2005, pp. 455-458.
[21] K. Wei, Z. Zhang, and Z. Feng, "Design of a wideband horizontally polarized omnidirectional printed loop antenna," *Antennas and Wireless Propagation Letters, IEEE,* vol. 11, pp. 49-52, 2012.
[22] J.-H. Park, Y.-H. Ryu, and J.-H. Lee, "Mu-zero resonance antenna," *Antennas and Propagation, IEEE Transactions on,* vol. 58, pp. 1865-1875, 2010.
[23] (2016, 5th March 2016). *Dipole Antenna* [Web]. Available: https://en.wikipedia.org/wiki/Dipole_antenna
[24] D. M. Pozar, *Microwave engineering*: John Wiley & Sons, 2009.
[25] D. J. P. Donohoe. (23 rd February). [Web]. Available: http://my.ece.msstate.edu/faculty/donohoe/ece4990notes5.pdf
[26] (2016, 17th March 2016). *Microwae Vision Group* [Web]. Available: http://www.mvg-world.com/products/field_product_family/antenna-1/electric-sleeve-dipoles